POLITECNICO DI MILANO

School of Industrial Engineering and Information

Master of Science in Materials Engineering and Nanotechnology

Characterization of ultra-light metal-polymer sandwich composite material through dynamic mechanical thermal analysis and microstructural analysis of nickel metal coating obtained through pulse-electrodeposition

Advisor**: Prof. Laura Vergani**

Assistant supervisor: **Dr. Roland Kádár**

Graduation thesis of:

Antonio Mulone ID N° 798558

Academic Year 2013/2014

Table of contents

List of figures

List of Tables

Abstract

The properties of a polymer-metal sandwich composite are investigated. The main scope of this project is a broad characterization of the sandwich material, performed in three branches: (i) investigation of the thermorheological properties and damping performance of the polymeric core, (ii) bending stiffness and core shear rigidity measurements, (iii) characterization of an electrodeposited nickel coating.

Different sandwich designs are tested: two facing materials, i.e. aluminium and stainless steel and two adhesives, i.e. a two and a single component epoxy based adhesives. The temperature influence on the mechanical response and its integrity is analysed through temperature ramp and frequency-temperature sweep rheological measurements. An analysis of the sandwich damping properties over a broad range of frequencies is performed through the application of the time-temperature superposition principle. Regarding the mechanical characterization, the first-order shear analysis is applied in order to calculate the bending stiffness and the core shear modulus of the sandwich materials. The measured values obtained loading the material under a three-point bending static test are then compared to the expected values from the thin-face approximation.

The results of the performed tests reveal operating limits for the samples characterized with the two components epoxy adhesive, after reaching temperature 20-30°C in excess of the measured adhesive glass transition temperature, T_g. Delamination of the metallic facing from the polymeric core occurs in such conditions. The samples characterized by the single component epoxy adhesive weren't instead affected by the same problem. From the mastercurves built applying the time temperature superposition principle, the frequency range for the investigation of the sandwich damping performances is extended beyond the measurable with conventional dynamic mechanical tests. The first-shear order analysis applied, allows a first evaluation of the sandwich core shear modulus.

The electrodeposition of a thin nickel layer on the metal facing of the sandwich composite is performed as a possibility to further enhance the mechanical performance of lightweight structures. The obtained nickel layer is characterized with electron back scattered diffraction, EBSD, and transmission electron microscopy, TEM, analysis in order to evaluate the grain size, grain size distribution, and their crystallographic orientation. Nanoindentation tests are then performed to measure the nickel Vickers hardness.

Abstract

Il seguente progetto di tesi tratta la caratterizzazione di un materiale composito a sandwich ultraleggero. Il materiale studiato è costituito da facce metalliche, e da un nucleo polimerico. Lo scopo principale della seguente ricerca è un'ampia caratterizzazione del materiale in analisi, sviluppata principalmente in tre diverse direzioni: (i) studio delle proprietà termo-reologiche del nucleo polimerico, (ii) misura della rigidezza flessionale e a taglio, (iii) caratterizzazione di un rivestimento di nichel ottenuto attraverso elettrodeposizione.

Del seguente materiale sono state considerate due diverse tipologie di facce metalliche (acciaio inossidabile e alluminio), e due adesivi epossidici, (un adesivo bicomponente e un adesivo monocomponente). L'effetto della temperatura sulla risposta meccanica e sull'integrità strutturale è determinato con prove termo-dinamiche meccaniche. In particolare sono condotte prove a rampa termica (*temperature ramp test)*, e a rampa di frequenza (*temperature frequency sweep test)*. La prima tipologia di prove ha permesso di valutare la temperatura di transizione vetrosa, T_g, dei diversi adesivi testati. Dai risultati ottenuti invece dalle prove a rampa di frequenza, attraverso l'applicazione del principio di sovrapposizione tempo-temperatura, le proprietà di smorzamento acustico del materiale sono valutate in un ampio spettro di frequenze. Per quanto concerne la caratterizzazione meccanica, questa è stata svolta attraverso prove statiche di flessione a tre punti. Considerando la totale deflessione, contenente anche i contributi relativi agli sforzi a taglio, è possibile valutare la rigidezza flessionale dell'intera struttura, e la rigidezza a taglio del nucleo polimerico. I valori di rigidezza flessionale, così ottenuti, sono poi confrontati con valori previsti analiticamente.

I risultati ottenuti dalle prove termo-dinamiche meccaniche evidenziano limiti di applicazione per i campioni caratterizzati con facce in acciaio inossidabile e con adesivo epossidico bicomponente, a temperature superiori di 20-30°C rispetto alla sua temperatura di transizione vetrosa. In queste condizioni si registra la delaminazione delle facce metalliche dal nucleo polimerico. Il fenomeno della delaminazione non è invece riscontrato per i campioni caratterizzati con l'adesivo monocomponente.

L'applicazione del principio di sovrapposizione tempo-temperatura ha permesso di estendere l'intervallo di frequenza per la valutazione delle proprietà di smorzamento del

composito a sandwich oltre i limiti imposti dalla strumentazione sperimentale. I risultati ottenuti mostrano, per i campioni di sandwich caratterizzati con l'adesivo monocomponente, proprietà di smorzamento acustico comparabili con quelle di polimeri amorfi, comunemente impiegati in compositi e strutture ibride per smorzamento acustico.

L'approccio sperimentale adottato per le prove meccaniche ha invece reso possibile una prima valutazione delle caratteristiche meccaniche del nucleo polimerico. I valori più elevati di rigidezza a taglio sono registrati per i campioni con adesivo monocomponente.

L'elettrodeposizione di un rivestimento di nichel sulle facce metalliche del composito a sandwich è effettuata come tentativo per aumentarne le proprietà meccaniche. Questa tecnica di deposizione permette l'affinamento delle dimensioni dei grani del materiale elettrodepositato, cui si accompagna un rafforzamento delle proprietà meccaniche del materiale. Per accertarsi delle caratteristiche microstrutturali dello strato di nichel si sono svolte prove di caratterizzazione superficiale attraverso microscopia elettronica. Si è utilizzato in particolare microscopio elettronico a scansione, SEM, con rilevatore di elettroni retro diffusi, EBSD, per misurarne la distribuzione granulometrica, e l'orientazione cristallografica preferenziale dei grani ottenuti. L'analisi condotta attraverso l'uso di microscopio elettronico a trasmissione, TEM, ha permesso di valutare le dimensioni di grani inferiori a 100 nm. I risultati ottenuti dalla caratterizzazione superficiale hanno evidenziato una granulometria non omogenea: pochi grani con diametro nell'intorno del micron circondati da grani più piccoli, la maggior parte con diametri compresi tra i 200-400 nm. Le immagini ottenute attraverso il TEM mostrano inoltre la probabile presenza di grani con dimensioni minori ai 100 nm. I risultati ottenuti dalla caratterizzazione superficiale sono confermati dai risultati delle prove di nanoindentazione svolti sul layer di nichel. I valori misurati della durezza di Vickers sono infatti comparabili con quelli attesi da nichel elettrodepositato con granulometria nell'intorno di 100 nm.

1 Introduction

In this first chapter and overview about composite materials, how they are classified and their application in the market is provided. The attention is in particular focused on lightweight sandwich materials.

1.1 Composite materials and their application

With composite materials we can refer to a very broad class of materials that can be both produced or found naturally, such as e.g. like wood or bones. Finding then a definition that could properly fit for all could be a quite challenging task. We can however say that a composite material is generally made by combining two or more constituents, often characterized by very different physical-chemical properties, which when combined, work together to give to the produced material characteristics different from those of the individual components. It is common to combine for example a strong and stiff material, distributed within another kind of material, instead softer and more ductile. The ductile constituent will work so as a matrix while the other, or the others if more than one, will act as reinforcement. The final properties of the product will be then influenced by the ductile matrix nature with an enhanced strength thanks to the stiffer reinforcement. Composites materials are in fact prepared in order to obtain desirable properties which could not be achieved by either of the constituents acting alone[1]. This possibility to combine different kind of matrix materials, with different type of reinforcement, varying the material itself, its composition, or just its geometry, allows to almost freely design the final desired properties[2]. This is what has made composite materials so attractive, starting from the more known fibres reinforced laminates, following with light weight structure, up to the latest possibilities opened up with nanostructures[3]. The reasons why composite are taking over with respect to conventional material in the aerospace field is related to the materials outstanding performance, regarding fatigue and corrosion resistance, and of course reduced costs[4]. The structural weight saving, obtained replacing metallic parts with lighter materials, leads to fuels saving, lowering then the overall cost. The aerospace market is probably the more relevant but the range of applications where the presence of composite material is strong is very large. The following table can provide a list of the other main applications:

INDUSTRIAL SECTOR	APPLICATION	COMPOSITE TYPES
Aerospace	Aircraft components: leading edges, ailerons, vertical stabilizers, wings, brake discs	Advanced composite materials(ACM), ceramic and metal matrix materials (CMC, MCM)
Naval	Racing boats, hovercrafts, canoes, pleasure boats, rescue crafts, trawlers	Fibres reinforced composite(FRC), sandwich structures
Automotive	Body panel, bumpers, brakes, drive shaft, wheels, cabins, seats, radiators grills	FRC, sandwich structure
Electrical and electronics	Insulators, cable tracks, antennas, batteries	Polymer matrix composite (PMC), polymer nanocomposite
Sports and goods	Tennis and squash rackets, skis, golf clubs, roller skates, bicycle frames, ice-hockey sticks	FRC
Medical	Implants	MMC, CMC

Table 1.1: Specific composite materials applications in different industrial sectors[4]

The design flexibility gained working with composite materials doesn't make designing a proper product for a particular application an easy task. Choosing between different class of materials to use as matrix or reinforcement, the composition and the structure of them, leads to different properties. Different aspects must be taken into account when designing a composite material. The difficulties that are usually incurred are mostly related to the definition itself of a composite material: a heterogeneous system. This intrinsic heterogeneity generates in most of the composites an anisotropic behaviour. This can be easily observed in unidirectional fibres reinforced composites, where of course the strength and the stiffness are much greater along the direction of the reinforcement. The relationship between stress and strains for anisotropic composites is also much more complex than it is for conventional isotropic materials. Here we can register coupling phenomena due to the combination of different loading modes[5].

1.2 Composite materials classification

Composite materials can be classified in different ways: depending on the kind of matrix material used, the kind of reinforcement and the overall composite design. Regarding the type of matrix used we can distinguish three different classes: polymer matrix composites (PMC), metal matrix composites (MMC), and ceramic matrix composites (CMC). PMCs has been dominating the other two classes in the market thanks to their wider application range, from structural to technological[4]. Polymer based composites are usually also characterized by a less demanding fabrication processes, in the sense of both less complex processing steps involved and cheaper raw materials needed. Nevertheless the other two classes find their application where the high performances and properties, not obtainable with PMCs, can justify the added cost[6][7] (e.g. aircraft components, space systems, combustion engines, sports equipment).

Several type of reinforcement can be used, whose use change depending on the properties to exploit. The reinforcements differ to each other depending from the kind of material used, their size and shape or their distribution within the matrix. A simple classification is provide in figure 1.1

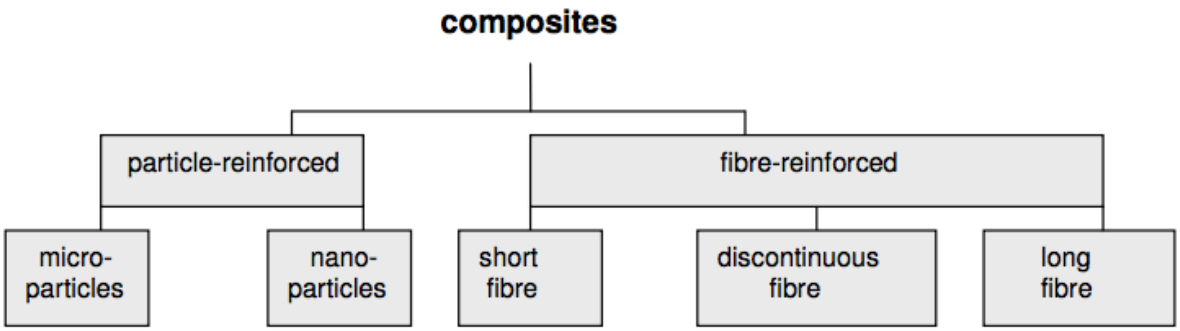

Figure 1.1: Composite classification depending on type of reinforcement

Regarding instead the overall composite design the attention will be focused just on the type of composite structure analysed in this thesis project: sandwich materials. A description of the characteristic features of this composite is provided in the next paragraph.

1.3 Sandwich structure

Among the different design possibilities for composite materials sandwich structures are becoming increasingly popular. The sandwich technology offers an enhancement in lightweight performance of composites that is of great interest for weight critical structures as airplane and naval parts, racing cars and sporting goods[8]. A sandwich composite is characterized by three distinct components: 1) two relatively thin and parallel sheet, of a stiff and dense material, called facing or skins of the sandwich; 2) a thick and lightweight core in between; 3) an adhesive layer which able to transfer the loads from the facing to the core and which has to ensure the integrity of the structure. The facing materials are mostly responsible for the bending loads of the overall structure. Common materials used are light metals, as aluminium or steel, or fibre reinforced composite laminates. The core of a sandwich composite represent in the same time the weaker part of the overall structure, and the component which minimize the weight with respect of solid body panels. Required properties for the core to ensure then good structural performances are low density, high shear modulus and shear strength, thermal stability, good fatigue and impact strength performances. Different types of core configurations and materials can be used to achieve these requirements, the most common are represented in figure 1.2. The categories in which they are commonly classified are: honeycomb, foam, web structure and balsa. Recently some hybridized structures have been developed where the core is made of glass fibre/epoxy or aramid fibre/epoxy laminae and the skins are made of aluminium alloy, leading to high performances which suits for aerospace applications, an example is provided by GLARE and ARALL composites[9][10][11]. A list of core properties depending on the type of material and core configuration is given in the following table 1.2.

Core material	Density Kg/m^3	Shear modulus MPa	Shear strength MPa
Aluminum honeycomb	70	460 (L) 200 (T)	2.2 (L) 1.5 (T)
Nomex honeycomb	80-129	69-112 (L) 44-64 (T)	2.2-3.2 (L) 1-1.7 (T)
Paper honeycomb	56	141 (L) 38 (T)	1.3 (L) 0.48 (T)
PVC foams	100-130	40	1.4-1.5
PUR foams	40	4	0.25
Balsa wood (SB50-100)	100-151	110-157	1.91-2.94

Table 1.2: List of properties for common core structures[8]

Honeycombs are natural or man-made structures with honeycomb geometry: hollow cell formed between thin vertical walls. The cells can have different shapes like rectangular, square, but the most common is the hexagonal. Several materials can be used for honeycomb cores: aluminium, carbon or glass fibres reinforced polymer (FRP), or Nomex, which refers to meta-aramid fibres, impregnated with phenol-formaldehyde. Generally this kind of design is hard to handle and quite expensive for some applications. Honeycomb sandwiches are mostly used for aircraft cabins or as sports goods, sailing racing boats or furniture. Web core is a structural core that consists in a continuous web, made of a solid material. This is formed in such a way that separates the two facing and it's really effective in transferring the shear forces[8].

With foams we refer to a system made of a solid matrix and a fluid, usually a gas. Foams are distinguished as open and closed-cell foams. In the closed form the gas is completely surrounded by the solid material and forms discrete cavities. The open foam is instead characterized by interconnected cavities. As for the honeycombs case, different kind of materials can be used, but the more common are polymeric foams, such as polyvinyl chloride or polyurethane, or light-metal foam, mostly aluminium.

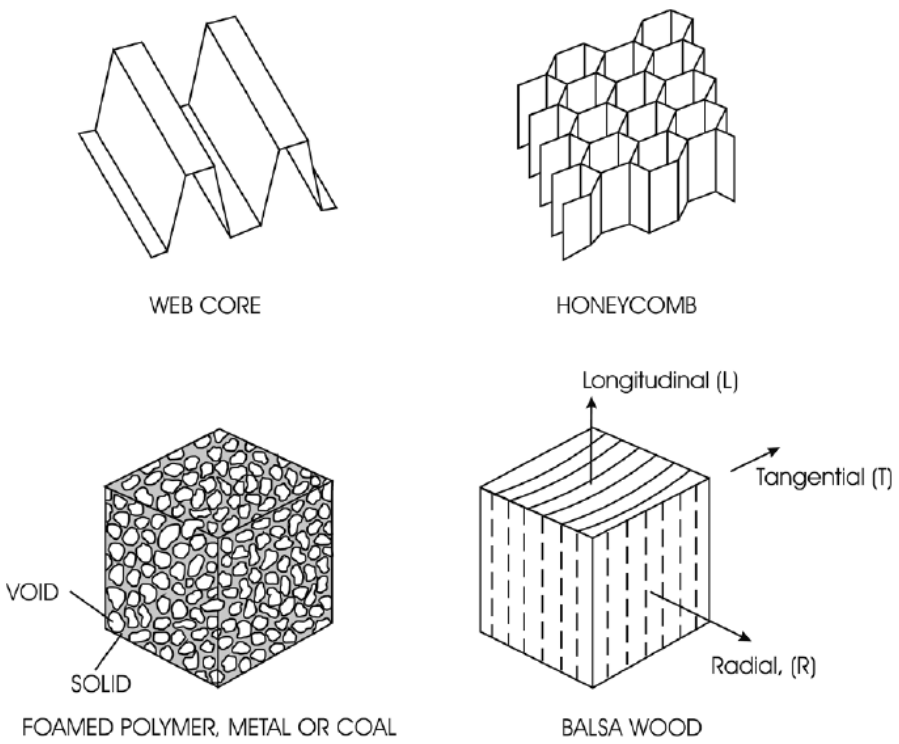

Figure 1.2: Different core structures

The most commercial are the polymer foams. Good thermal-electrical insulation, acoustic damping, and lower prices characterize these types of sandwich materials. These structures are used mostly in automotive or naval applications, or in other fields that require moderate structural properties, or as disposal packaging.

Balsa is a natural wood product and is a moderately priced core material but it can suffers of water intake problems even if it has an higher density than the other types of structural cores. An overall view for the described core structures, regarding the cost versus their performances is shown in fig 1.3.

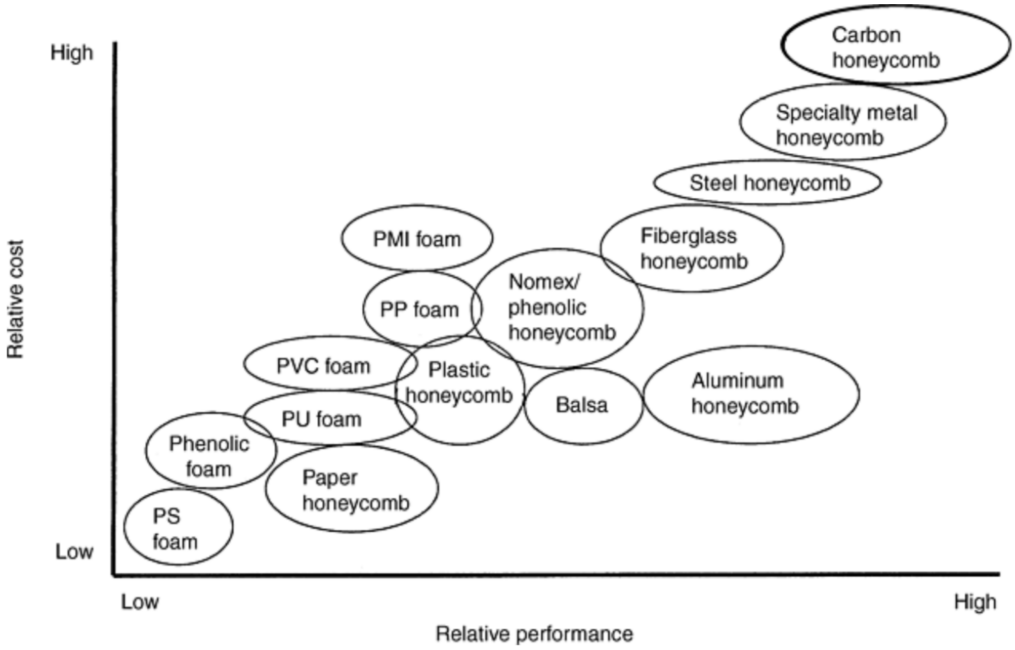

Figure 1.3: Plot showing the relative performance of different core designs with respect of their cost[12]

The sandwich material subject of analysis in this thesis is hard to classify within one of the described structure. Its unique design is patented and owned by Lamera AB, a company operating in the lightweight material design and development. A description of the company and of the material tested is given in the following chapter.

2 Hybrix™

In this chapter the sandwich material investigated in this thesis is described. The company producing the composite material and its manufactory process is also briefly reported. Finally the previous work done on the material and the goals of this study are presented.

2.1 The company: Lamera AB

Lamera AB is a spin off company from Volvo Technology founded in 2005. The company is located in Gothenburg, Sweden. The manufacturing of the sandwich composites takes place at a pilot plant in Tibro, Sweden. Lamera AB focuses on design and weight oriented customers mainly within the aircraft, railway, automotive fields as well as exclusive customer's good. The main lightweight material produced is the sandwich Hybrix™.

2.2 The product: Hybrix™

The Hybrix™ is a metal sandwich characterized by two thin metal sheets facing and with a core of polymer or metal fibres attached to the facing through an adhesive layer, see fig. 2.1. The unique configuration of the fibres, aligned perpendicular before they are compressed between the two layers, leads to final configuration with an open core structure. Thanks to the Hybrix™ air-rich core the weight reduction is estimated to be up to 35-60% in comparison to solid sheet metal of equal dimensions. Lamera AB promote also Hybrix™ sandwich for its excellent forming properties. It can be shaped using the same machinery tools as for solid sheet material[13],as those listed in fig 2.2. Hybrix™ applications are primarily within the automotive sector, and other transport-related markets. Here, Hybrix™ aims to replace solid metallic components commonly used.

Figure 2.1: Hybrix™ cross-section showing the different constituents: i.e. metal facing, adhesive layer ad polyamide 6,6 fibres

Different Hybrix^{TM} configurations can be produced. The facing can be of stainless steel or of lighter metal like aluminium. Regarding the core, the production was first focused on the development of Hybrix^{TM} sandwich with stainless steel fibres. But the price of the final product holds for making it competitive in the market. To overcome this problem the production of a sandwich with polyamide 6,6 fibres was developed. The facing thickness and the core size can also be varied in order to obtain the best design configuration to best suit the customer's requirements. The adhesive layer used nowadays is a two component epoxy based glue, referred from the company as adhesive B. Recently a new adhesive has been developed, a single component epoxy based, referred ad adhesive C. Due to trade market company policy further specifications about the adhesives can't be provided.

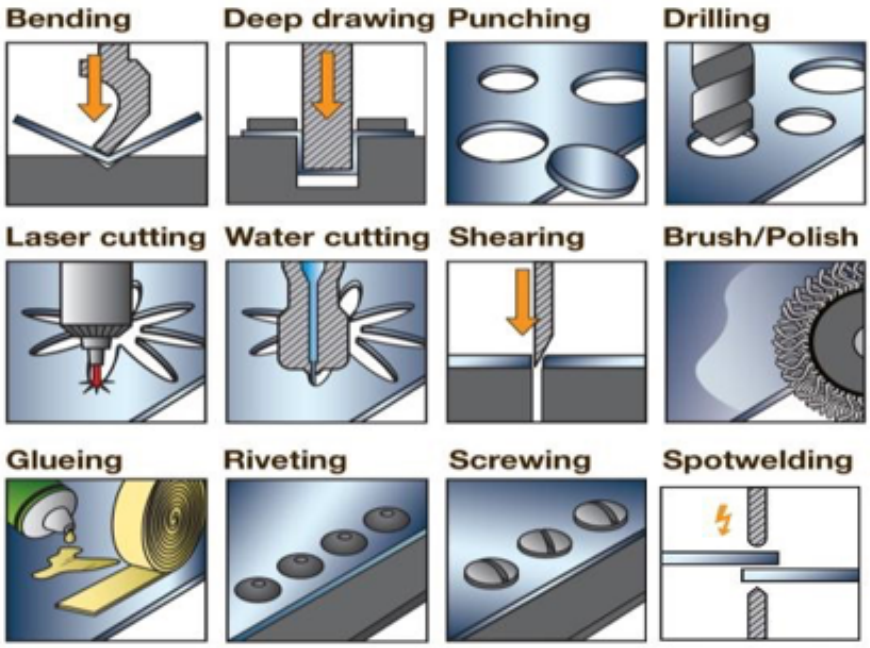

Figure 2.2: Possible shaping methods applicable for Hybrix^{TM}

2.3 Manufacturing process

The production of Hybrix^{TM} is characterized by different steps: (i) adhesive deposition on the facing, (ii) fibres deposition in the electrostatic flocking station, (iii) curing of the assembled product, (iiii) quality check and cutting/shaping of the product[14]. The metal sheets facing, with a thickness between 50-200 µm, are covered with a 200 µm adhesive layer, applied through rollers coaters. Once the adhesive is applied, one of the metal sheets is moved to the electrostatic flocking station where it is flocked with fibres. Applying an

electric field during the process, the fibres with a negative charge and the metal sheet grounded, lead to a vertical disposition of the fibres on the metal facing. After all the fibres have been attached in this way onto the adhesive layer, the other metal facing is put on top with the adhesive layer side against the fibres. The obtained structured is afterwards cured and pressed up to 60% of its original thickness. The last step is the quality check and just after that the sandwich is cut to the desired size and ready for the market[14].

2.4 Previous work

The first sandwich samples were produced when Volvo owned the Hybrix^{TM} technology, the production was small and focused only on the design with stainless steel facing and fibres core. After Lamera AB bought the Hybrix^{TM} technology a pilot factory for the production was built up. After 2009 the product was optimized, testing a new type of adhesive, aluminium facing and polyamide fibres. In 2011 Jon Wingborg carried on at Chalmers a thesis project, in collaboration with Lamera AB, based on the Hybrix^{TM} sandwich. The project was focused mainly in two aspects. A market analysis was conducted first, in order to detect the possible material applications, based on a comparison of the Hybrix^{TM} bending stiffness with the competitors material, solid aluminium and stainless steel. The second step aimed to test different kind of adhesives that could ensure a good formability of the product, and an increase of the bending stiffness, in order to make the Hybrix^{TM} product an attractive alternative to solid sheet metals. After testing up to 25 different adhesives just one could fulfil both requirement. This is the two component epoxy based adhesive which is used today, adhesive B. Within the same project the adhesive was tested in different sandwich configuration: carbon steel and aluminium facing, stainless steel and polyamide fibres.

2.5 Material code for Hybrix^{TM}: tested samples

In this thesis project both aluminium and stainless steel facing Hybrix^{TM} have been tested. The facing thickness was 0,15 mm for all the samples characterized with the stainless steel facing, while 0,2 mm for the aluminium. The Hybrix^{TM} panels provided by Lamera AB were characterized with three different mixing ratio of the two component epoxy adhesive B, and different core thicknesses. Just one panel with stainless steel facing was provided with the new adhesive C. The polyamide fibres length in all the samples was of 2 mm.

In this thesis project to distinguish the different samples these will be named as follows: the first letter of the code stands for the facing metal, i.e. S= stainless steel or A= aluminium; the second letter to the kind of fibres in the core, P= Polyamide. To distinguish between samples characterized by different adhesive a last letter is added to the sample name. For the adhesive B a distinction between the different mixing ratios used will be provided as follow: B(r:h_i). The "r" within the bracket stands for "resin", while "h" for hardener. The subscript "i" will range from 1 to 3. The exact amount of the component is not provided due to trademark restrictions. A clarification of the adopted code is provide as follow:

- APB(r:h_i)
- SPB(r:h_i)
- SPC

In this case then first code will refers to a sample characterized with aluminium facing, polyamide fibre, and adhesive B with a defined mixing ration. The same can said for the second sample, the only difference is represented by stainless steel as facing material. Stainless steel facing, polyamide fibres and adhesive C characterize the third sample. A table with the specifications of all the tested Hybrix^{TM} samples here follows:

Material/sample code	Facing thickness (h_f), mm	Core thickness (h_c), mm
APB(r:h_1)	0,2	0,6
SPB(r:h_1)	0,15	0,7-1,35
SPB(r:h_2)	0,15	1,25
SPB(r:h_3)	0,15	0,7-1,25
SPC	0,15	1,1

Table 2.1: Specification of sandwich sample tested

2.6 Description of the project

The main scope of this project is a broad characterization of Hybrix^{TM}. This is performed in three branches: (i) investigation of the thermorheological properties and damping

performances of the polymeric core, (ii) bending stiffness and core shear rigidity measurements, (iii) characterization of an electrodeposited nickel coating.

The analysis of the thermorheological properties is performed through dynamic mechanical thermal analysis, DMTA, and is presented in the third chapter. The glass transition temperature, T_g, of the different adhesives is measured with temperature ramp tests. Temperature-frequency sweep tests are performed instead for measuring the material damping performance. As an attempt to investigate the damping properties over a broad frequency window, the time-temperature superposition is applied. The tests results and the following conclusions are presented in the same chapter.

Chapter 4 focus instead on the evaluation of the mechanical properties of the sandwich material tested. Here bending tests under 3-point bending are performed according to the first-order shear analysis in order to have a first evaluation of Hybrix^{TM} core shear stiffness.

The last chapter describes instead the electrodeposition of a nickel coating on the stainless steel facing of Hybrix^{TM}. This technique is performed as a first attempt to improve the properties of lightweight materials. Mechanical properties such as Vickers hardness and yield strength are strongly influenced by the material microstructure. A refinement of material grain size corresponds to a sensible increase in both mechanical properties. In this sense, the possibility offered by the electrodeposition technique to control the grain size and grain distribution, represents a powerful instrument. Materials characterized by nanocrystalline grains achieve highest performance. The deposition is performed through pulspe-electrodeposition with a nickel sulfamate solution. The nickel layer obtained is characterized both by microstructural analysis and mechanical test, i.e. Vickers Hardness measurements.

The last chapter provides a summary of the obtained results, the conclusions and potential future developments that may follow.

3 Dynamic Mechanical Thermal Analysis

The main aim of these tests is the evaluation of the temperature influence on the adhesives and also on the nylon fibres present in the Hybrix^{TM} core. The adhesives thermal behaviour is crucial for sandwich composites in order to ensure a proper structural integrity. In particular for metallic facing that combined with polymer can suffers of low interfacial strength[15]. Thus, to investigate the viscoelastic response of the Hybrix^{TM} Dynamic Mechanical Thermal Analysis (DMTA) tests were performed. In the first paragraph, a brief description of the principles of dynamic testing and the viscoelastic properties measurable in such testing conditions is provided. Following with the experimental measurements of the adhesive glass transition temperature, T_g, through temperature ramp tests. The damping properties are instead measured through temperature-frequency sweep tests, applying the time-temperature superposition principle.

3.1 Dynamic mechanical tests on viscoelastic materials: characteristic features

Testing a sample under dynamic mechanical tests, the applied input, i.e. stress or strain, can be expressed in a sinusoidal wave form:

$$\varepsilon(t) = \epsilon_0 \sin \omega t \quad \text{(eq. 3.1)}$$

$$\sigma(t) = \sigma_0 \sin \omega t \quad \text{(eq. 3.2)}$$

If the tested specimen can be considered as a perfect elastic body, assuming as input a sinusoidal strain, eq. 3.1, the material response would be given simply by eq. 3.2. For an ideally viscous material instead, the response would be deleted of π/2 radians:

$$\sigma(t) = \sigma_0 \sin\left(\omega t + \frac{\pi}{2}\right) \quad \text{(eq. 3.3)}$$

Polymers materials behave in between a perfectly elastic and a perfectly viscous material. Due to this intrinsic characteristic, their response to a sinusoidal applied strain is described as[16]:

$$\sigma(t) = \sigma_0 \sin(\omega t + \delta) \quad \text{(eq. 3.4)}$$

A graphical representation of the different material response to the applied input is given in fig. 3.1.

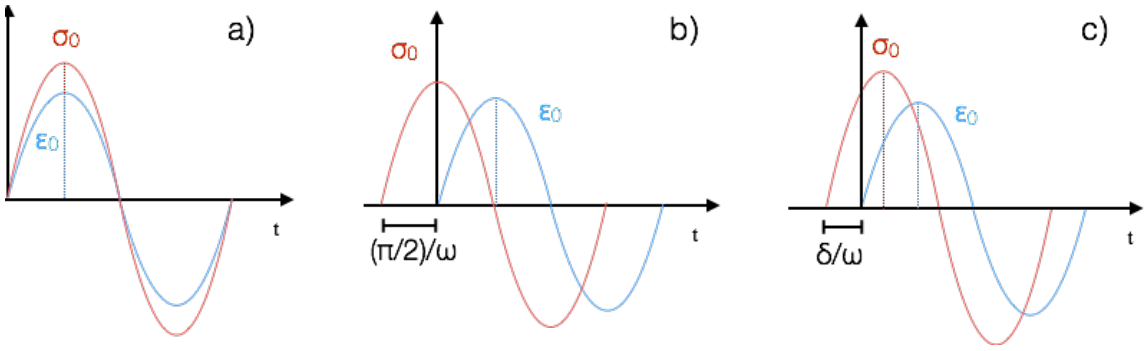

Figure 3.1: Material response in case of perfectly elastic material a), perfectly viscous material b), viscoelastic material c)

If we express now the material modulus in is complex form as:

$$E^* = E' + iE'' = \frac{\sigma_0}{\varepsilon_0}(\cos\delta + i\sin\delta) \qquad \text{(eq. 3.5)}$$

E' is defined as the storage modulus, which represent the conservative component of the overall complex modulus E^*. E'' is instead the loss modulus, the dissipative component of the complex modulus. If the storage modulus E' stands for the elastic response of the material, the viscoelastic behaviour is depicted by the loss modulus E'', or by the ratio of the two quantity, which is defined as loss factor:

$$\tan\delta = \frac{E''}{E'} \qquad \text{(eq. 3.6)}$$

The glass transition temperature T_g and damping performance of a polymer or polymer-based composites are evaluated by the loss factor variation with temperature and/or with frequency. In particular, plotting tan δ vs. Temperature, a measure of the T_g is provided by the peak of the obtained curve. Another evaluation of the T_g can be also obtained from the inflection point of E' curve plotted always with respect of the temperature[17]. Figure 3.2 provides a representation of the two procedures.

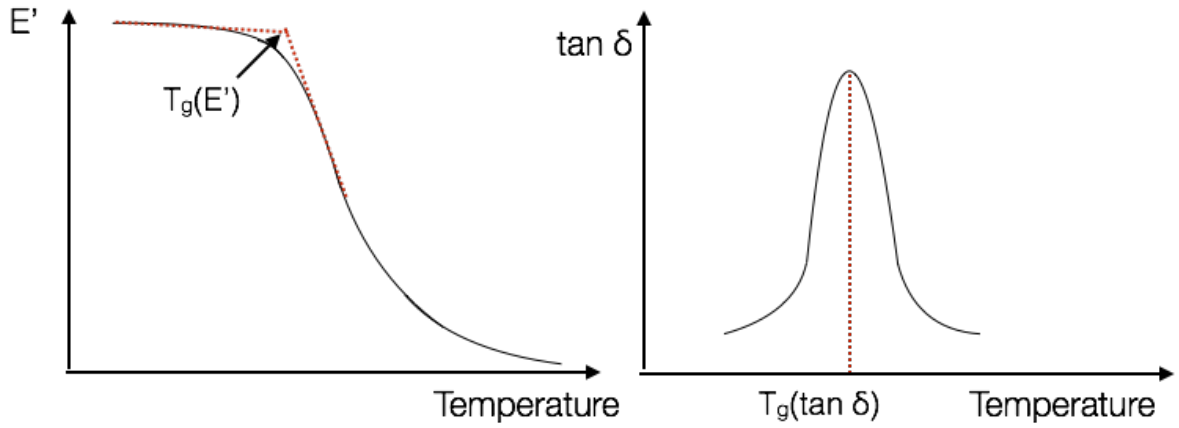

Figure 3.2: Schematic representation of T_g evaluation from storage modulus inflection point, and from tan δ peak

The determination of the T_g for a polymeric material is of fundamental importance. It represents the temperature at which the transition between the "solid" and "liquid" state occurs[16]. The "liquid" state of a polymer at temperatures above the T_g is simply represented by a higher mobility of its chains. In order for a polymer to actually flow higher temperatures are needed. However the higher mobility of the polymeric chain will strongly affect the material mechanical response.

3.2 Temperature ramp: tests and samples description

All the DMTA tests were performed on a Rheometrics RSA II in the Rheology Lab at Chalmers University of Technology. This device is mostly used to test softer materials like polymers, since it has a maximum force of 10 N, but it has proven to be suitable also for Hybrix™ samples. During preliminary investigation, different samples width, i.e. 8, 10 and 12 mm, and two different holding fixtures, i.e. three-point bending fixture and dual cantilever, have been tested. After these first trials to detect the suitability of the Rheometrics with composite samples, just samples of 10 mm width and 52 mm length were used, loaded under three-point bending. Two different cutting techniques were used to obtain the samples: shear cutting, and water jet cutting.

Temperature ramp test are performed applying a constant strain amplitude and a constant frequency, properly selected within the linear viscoelastic region of the investigated material, while progressively increasing the temperature at fixed rate, see fig. 3.3.

During the tests the change in the storage modulus E', loss modulus E'' and loss factor, tan δ is measured. To select the limit of the linear viscoelastic region, for each sample a dynamic strain sweep is first performed: the amplitude of the applied deflection is constantly increased, at a constant frequency. The test was repeated for each sample at four different frequencies: i.e. 1, 2,4, 5 and 10 Hz.

All the different Hybrix^{TM} samples were tested according to two different procedures:

- Procedure 1: dT/dt of 1°C/min, with T∈[30,100]°C for adhesive B samples, with T∈[30,130]°C for adhesive C samples. Selected frequency of 2,4 Hz. Air gas used as refrigerant.
- Procedure 2: dT/dt of 5°C/min, with with T∈[T_g-50,T_g+50]°C. Selected frequency of 1 Hz. Liquid N_2 used as a refrigerant.

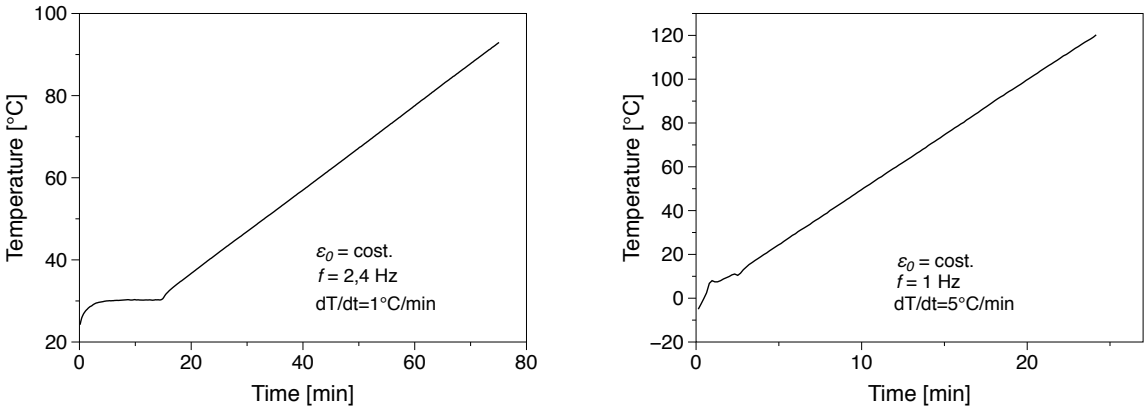

Figure 3.3: Temperature ramp tests performed through procedure 1 on the left, through procedure 2 on the right

Procedure 1 was set accordingly to the same condition at which the Hybrix^{TM} were previously tested[14]. Procedure 2 was instead set according to the standard ASTM D7028-"Standard Test Method for Glass Transition Temperature of Polymer Matrix Composites by Dynamic Mechanical Analysis". The list of the different tested specimen is reported in the table 3.1. The results and the conclusion that can be depicted are presented in the following paragraph.

Adhesive	Metal facing
B(r:h_1)	Both aluminium and stainless steel
B(r:h_2)	Stainless steel
B(r:h_3)	Stainless steel
C	Stainless steel

Table 3.1: Sample used for temperature ramp tests

3.3 Temperature ramp tests: experimental results and discussion

The first tests were performed, following procedure 1, on the Hybrix^{TM} samples APB(r:h_1) and SPB(r:h_1). This is the adhesive currently used for the production of Hybrix^{TM}. The starting temperature of 30°C was chosen because a proper control of the temperature rate, starting from lower temperatures, was not possible without using liquid N_2 as a refrigerant. The results of this first tested are showed in figure 3.4

Analysing the curves obtained from the aluminium facing samples the T_g of the adhesive from the peak of the tan delta can be easily evaluated at around 50°C. This value is slightly higher than the expected value from the company specifications (45°C), but will be confirmed by other tests conducted with the same adhesive, and same mixing ratios. Still regarding the measured T_g another aspect has to be considered: the polymeric core of Hybrix^{TM} sandwich tested is constituted of two distinct polymeric phases, characterized by two different glass transition temperatures, around 56°C for polyamide 6,6 and 45°C for the adhesive B(r:h_1). Being the measured T_g in between these two values, it is not possible to establish with certainty which of the two polymeric phases is more responsible fort the overall thermorheological behaviour of the sample. Especially considering that these were the first temperature ramp test performed on Hybrix^{TM} sandwich with nylon fibres. Regarding the E' modulus variation with temperature, as expected the decrease starts at temperatures close to the measured T_g and it gets almost the half of the value measured at room temperature at around 60°C.

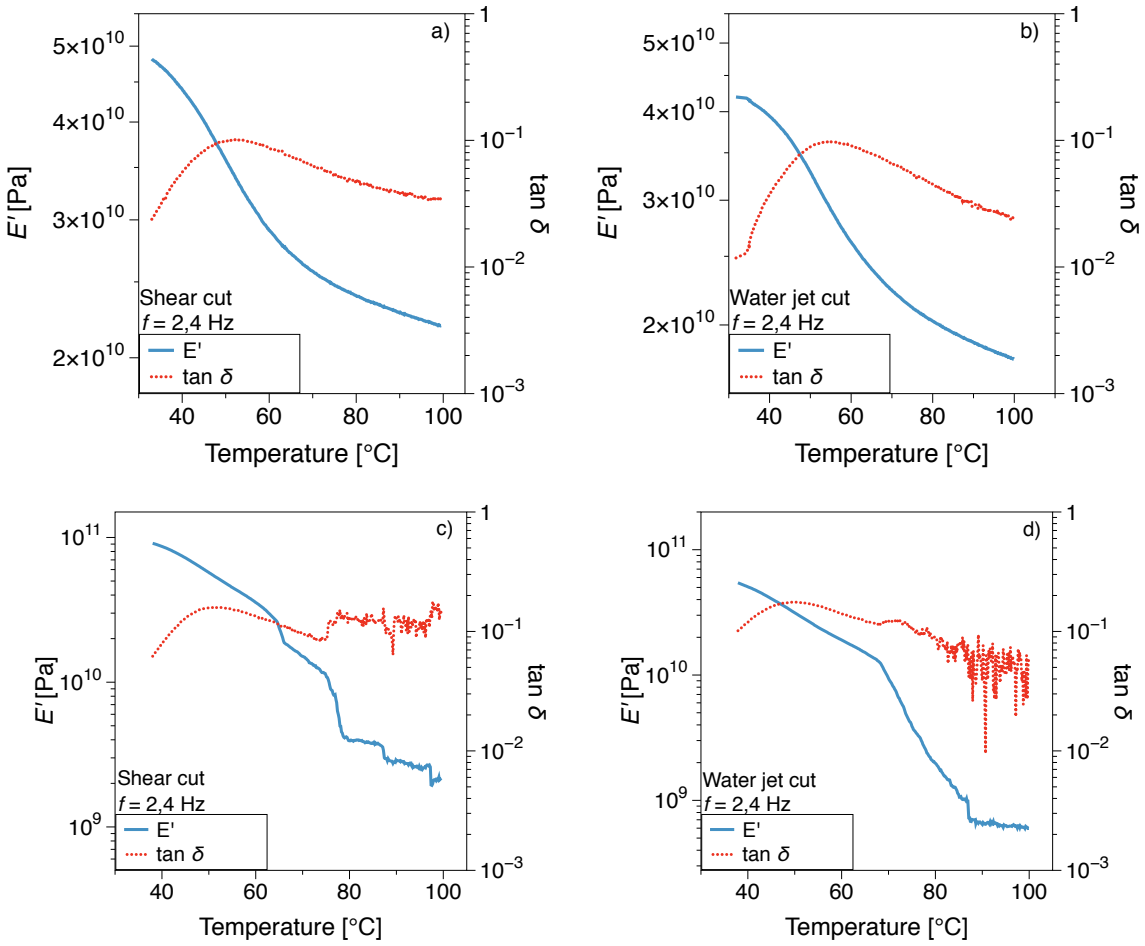

Figure 3.4: Temperature ramp results showing the storage modulus E' and the loss factor tan δ for APB(r:h_1) (a-b), and for SPB(r:h_1) (c-d)

Analysing instead the plots of the stainless steel facing samples, the first noticeable result is the delamination of the tested samples. This phenomenon is indicated in the plots by a sudden drop of the storage modulus, over one order of magnitude. The trend of the curve shows how the delamination starts probably at temperature higher than the measured T_g, and it propagates with the increasing temperature. This results, confirmed by other tests than the two reported, was unexpected from the company Lamera AB, and led to production of the other two Hybrix^{TM} configurations, still characterized with the adhesive B, but with two different mixing ratio. The comparison between the samples obtained with the two different cutting techniques was also performed to exclude any possible influence of the cutting technique, but as shown in figure 3.4 (d) water jet samples were as well affected by delamination.

To exclude also any improper production of the tested samples, causing an improper adhesion between the adhesive and the stainless steel facing, two other SPB(r:h_1) panels

were produced and delivered. In one, the metal facing, before the application of the adhesive layer, were cleaned with acetone, according to the usual production step, in the other one the cleaning was instead not performed. The samples tested from these new panels were however affected by the same delamination problem, the only detectable difference was that the delamination seems to start a slightly higher temperature and the effected area was less pronounced, mostly localized ad the samples edges, in the longitudinal direction. The different delamination length is showed in fig. 3.5.

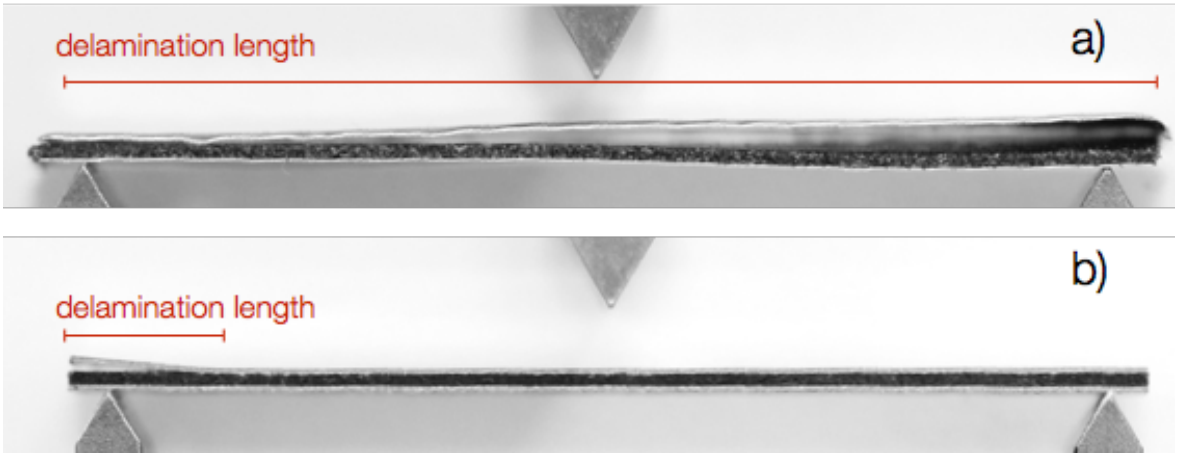

Figure 3.5: Hybrix^{TM} samples showing different delamination length: a) affecting the whole structure, b) localized just at the sample edge

For Hybrix^{TM} samples characterized with the new adhesives, SPC, SPB(r:h_2), SPB(r:h_3), the temperature ramp test were performed following both procedure 1 and procedure 2. The tested samples were all cut just through shear cutting since the applied cutting technique didn't prove to be a possible cause for the delamination phenomenon in the previous tests. Figure 3.6 shows the comparison of the plots obtained with both procedures. With the procedure 2 it was also possible to detect the T_g obtained through the intercept of two tangent line from the semi-logarithmic plot of E' vs. temperature. This T_g, lower than the one measured from the tan δ peak, provides information regarding the temperature at which the storage modulus starts to decrease, and thus at which temperature the mechanical properties start to be affected. The same information for the adhesive B(r:h_1) was provided performing a temperature ramp test following procedure 2 for an APB(r:h_1) sample, see fig 3.7.

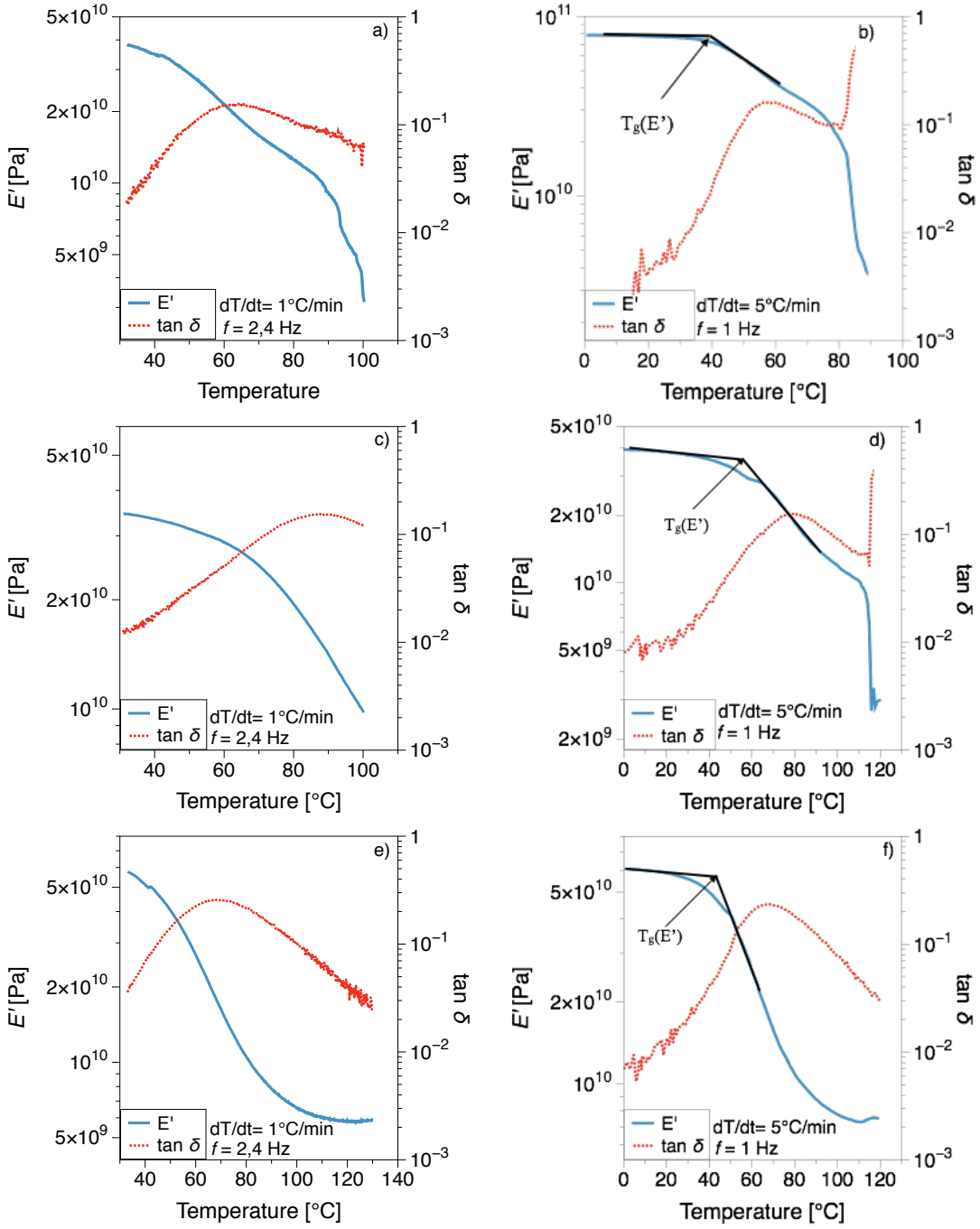

Figure 3.6: Temperature ramp results showing the storage modulus E' and the loss factor tan δ, from the comparison of procedure 1 and 2, for adhesive B(r:h_2) (a-b), B(r:h_3) (c-d), C (e-f)

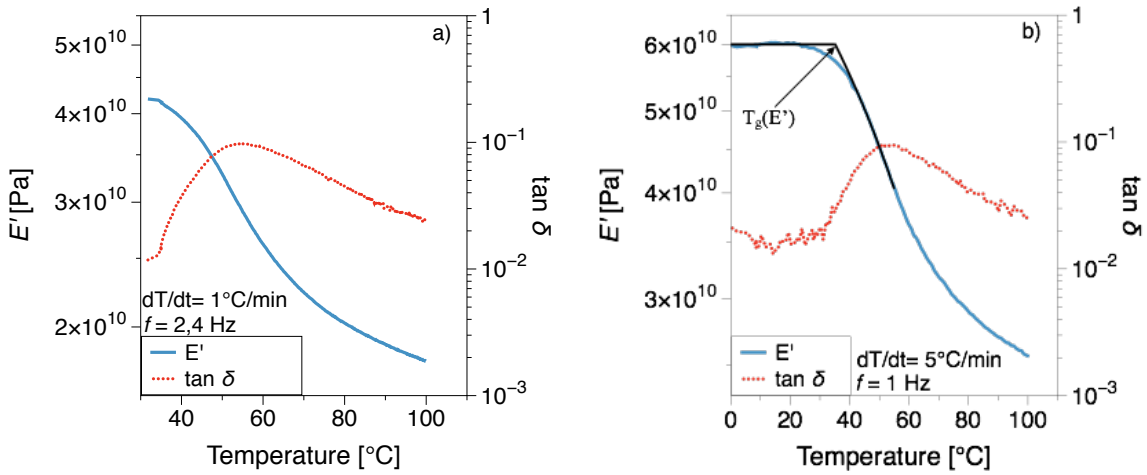

Figure 3.7: Temperature ramp results showing the storage modulus E' and the loss factor tan δ, from the comparison of procedure 1 (a) and 2 (b) for adhesive B(r:h_1)

Analysing the results obtained by the new temperature ramp plot several conclusions can be outlined. Regarding the integrity of the sandwich structure, it appears that all the stainless steel facing samples characterized by the two-component epoxy adhesive B, even with different mixing ratios, suffered of delamination. This phenomenon seems to occur at $T>T_g+25\pm5°C$, starting from the sample edge in the longitudinal direction and then propagating toward the centre, see figure 3.5. The influence of the different mixing ratio for the adhesive B led only to different values of the measured T_g. Delamination is not found however for the samples characterized with the one component epoxy adhesive C.

Unfortunately from the data available the cause for the delamination of the adhesive B samples cannot be assessed with certainty. A reasoning of the possible causes behind this phenomenon, considering the adhesion mechanism of composites materials, is provided in the following paragraph.

Looking at the tan δ curves for the adhesives characterized by the highest T_g values, B(r:h_3) and C, it seems evident that no peak is detected at temperatures close to the T_g of the nylon fibres, 56°C. Hence, temperature ramp tests conducted applying flexural loads seem to have a small or negligible effect on the nylon fibres present in the core. Two possible reasons have been identified as a possible explanation: (i) the contribution to the flexural stiffness of the Hybrix^{TM} sandwich given by the nylon fibres it's low, (ii) an high crystallinity of the polyamide fibres present in the core. According to the first conjecture under bending, the polymeric phase mostly responsible for a proper load transfer between

the two metallic facing is the adhesive layer. Furthermore being the Hybrix^{TM} sandwich characterized by low thicknesses, the adhesive layer could directly ensure the contact between the two metal facing, see figure 3.8, further decreasing the contribution given by the nylon fibres to the overall flexural rigidity of the composite. The other possibility is that the nylon fibres used are characterized by a high crystallinity. The temperature less affects polymers characterized by a high degree of crystallinity.

Figure 3.8: Stylized representation of Hybrix^{TM} core structure with proper separation of the metal facing (a), with local region of through-thickness epoxy adhesive (b)

As an attempt to verify the possibility of a different adhesive distribution, as the one hypothesized in figure 3.8, some pictures of the cross-section of the Hybrix^{TM} samples were taken through a digital scanning electron microscope (DSEM). These are showed in figure 3.9.

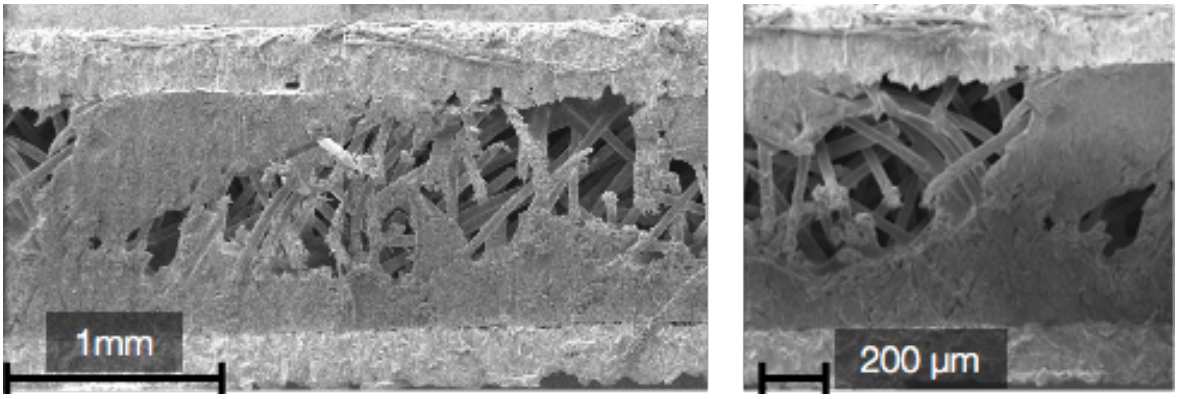

Figure 3.9: DSEM pictures of different cross-sections of Hybrix^{TM} samples

The two cross-section images, taken at different magnification, reveal some areas where the adhesive layer seems to be distributed over the whole sandwich thickness.

Regarding the assumption of a high crystallinity of the nylon fibres no information about the material were provided by the company, so it is not possible to confirm this hypothesis. The most probable explanation is that the fibres are less influenced with respect to the adhesives, with the applied testing condition. Other testing conditions, i.e. temperature ramp under shear, may lead to different results and clarifications.

3.4 Adhesion mechanisms

If the surfaces of two bodies come spontaneously into intimate contact the adhesion between the two surfaces is primarily caused by molecular attraction forces, van der Waals forces [5]. If one of the two materials is a fluid, the wettability of the solid surface has to be considered. As a matter of fact the wettability is the behaviour of a material with respect to a liquid by which is wetted. The common equation governing this phenomenon is the Young-Dupree eq. here reported:

$$\Gamma_{lv} \cos\theta = \Gamma_{sv} - \Gamma_{sl} \qquad \text{(eq. 3.7)}$$

Here Γ_{lv} stands as the surface tensions at the liquid/vapour interface, Γ_{sv} the solid/vapour, while Γ_{sl} the solid/liquid surface tension. Intimate contact in this case is provided if the liquid is not too viscous, and a thermodynamic driving force favours the process. The wetting at the equilibrium described by the Young's equation is shown in fig. 3.10:

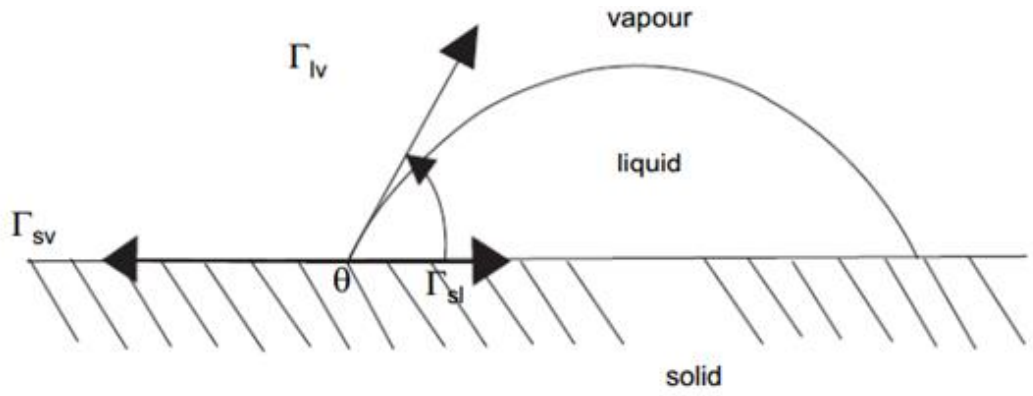

Figure 3.10: Wetting at equilibrium with surface tensions expressed as vectors

From Young's equation follows that complete wetting occurs for cos(θ) tending to 1, or when the wetting angle θ tends to zero. This can occur if the surface energy of the solid material is the same or greater than the sum between the liquid surface energy and the interface surface energy. Surface energies of liquid material are usually known from the scientific literature, the other two components of Young's equation can be measured by different wetting tests.

Van der Waals force are not the only occurring during adhesion, other type of bonding may reinforce the adhesion strength[5]:

- Interdiffusion and molecular entanglement
- Electrostatic attraction
- Chemical bonding
- Mechanical keying or interlocking

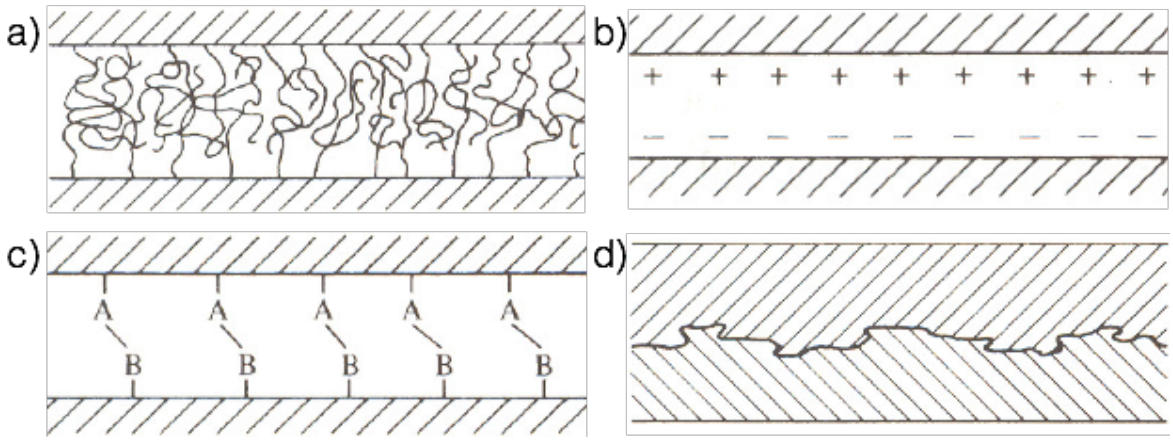

Figure 3.11: Adhesion mechanisms: a) interdiffusion and molecular entanglement, b) electrostatic attraction, c) chemical bonding, d) mechanical keying or interlocking

A schematic representation of the different adhesion mechanism is provided in figure 3.11. Adhesion between epoxy compounds and metallic surfaces is provided mainly by chemical or electrostatic attraction, and by mechanical keying[18]. The first two mechanisms are favoured by the presence of metallic oxide, causing an electrostatic interaction. The formation of chemical bonds occurs between active hydrogen in steel surface and the epoxide groups, or by bond dissociation between phenoxy oxide and carbon[19]. Mechanical interlocking is instead obtained specially in presence of rough surfaces, or porous oxides that allow the epoxy resin and curing agents to penetrate within the oxide voids.

For a proper investigation of the wettability of the metallic facing with respect of the two different adhesives, B and C, contact angle measurements are necessary. Due to the impossibility to handle the two different epoxy adhesive, separately from the other sandwich components, it wasn't possible to investigate this aspect.

However, roughness measurements of the two metallic facing, i.e. aluminium and stainless steel, were performed to determine any possible difference in the interlocking mechanism. Rougher surfaces may increase the epoxy interlocking within the metal voids. This will then enhance the strength of the adhesion of the two phases. The measurements were performed on the outer side of the metallic facing of the sandwich samples. A comparable roughness with the inner side of the metallic sheet is then assumed. Considering that the only pre-treatment of the metallic Hybrix^{TM} facing is cleaning process, through acetone rinsing, this assumption can be considered valid. The measurements were performed with a WYKO optical profilometer, RST plus model. The magnification used was 10X. The surface maps, both in 2-D and 3-D representation, are showed in figure 3.12:

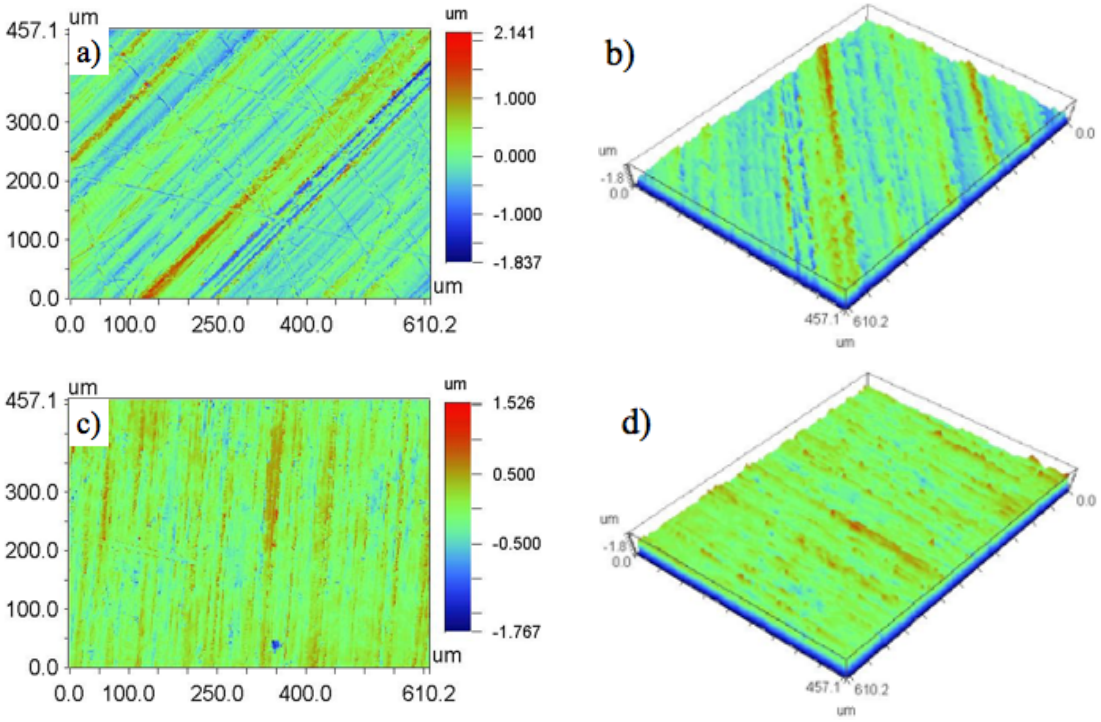

Figure 3.12: 2-D and 3-D representation of surface roughness for aluminium facing a) and b), 2-D and 3-D representation of surface roughness for stainless facing c) and d)

The results reveal a higher average surface roughness, Sa, for the aluminium facing, i.e. S_a= 0,27 µm, with respect of the stainless steel facing, i.e. S_a=0,18 µm. Such a difference could explain a better adhesion of the adhesive B registered with the aluminium facing. However, the lower roughness of the stainless steel facing doesn't represent a limitation when using the single component epoxy, adhesive C.

Furthermore, other aspects should be considered to proper investigate the delamination phenomenon. Since the delamination is incurred at relative high temperature, the thermal expansion coefficient mismatch between the different materials can also play a role.

As it appears the phenomenon is complex, and the effective cause of the delamination is probably represented by a combination of the presented conjectures, i.e. surface roughness, wettability of the different adhesives, thermal expansion mismatch. Further studies are needed in order to assess with certainty the cause of the phenomenon and to assess the different adhesion strength between the two different adhesives. However, the results here obtained, both from the temperature ramp tests and from the surface roughness measurement, can represent a starting point for further analysis.

3.5 Temperature ramp test: conclusion summary

From the results showed in the previous paragraphs, a list with the values of the measured T_g, for the different adhesives is provided in the following table:

Adhesive type	T_g (tan δ)	T_g (E')	Delamination
B(r:h_1)	50°	35°	For T≃70°
B(r:h_2)	60°	40°	For T≃85°
B(r:h_3)	80-85°	60°	For T≃110°
C	68-70°	45°	Not incurred

Table 3.2: Loss factor values for the different tested samples

A short summary of the conclusion obtained after the performed tests are here listed:

- Hybrix^{TM} samples with stainless steel facing characterized by the adhesive B, independently of the applied mixing ratio for the epoxy components, suffered of delamination.
- Hybrix^{TM} samples characterize by the adhesive C weren't affected by delamination
- The nylon fibres, polyamide 6,6, present in the Hybrix^{TM} core seems to be not detected with the testing condition applied: temperature ramp with flexural load.

- A higher surface roughness of the aluminium facing, enhancing the interlocking of the adhesive layer, can provide a possible reasoning for a higher strength of the adhesive B - aluminium bonding.

3.6 Temperature-Frequency sweep: test and sample description

In order to obtain more information about the damping performance of the Hybrix^{TM} material, and its dependence on the frequency, for the samples that show a good integrity and don't exhibit any delamination problem, temperature frequency sweep tests were performed. Hence only two type of adhesives have been tested, adhesive B(r:h_1), with aluminium facing, and adhesive C, with stainless steel facing. The tests were performed with the same DMTA, Rheometrics RSA II, described in paragraph 3.2, and with the same holding fixture, 3-point bending.

During a temperature-frequency sweep the temperature is raised to some selected steps and here kept constant. Within these steps, after a soak time in order to reach a temperature equilibrium, a frequency sweep is performed: with a constant strain amplitude applied, the frequency is continuously varied within a selected range, measuring meanwhile the thermorheological properties of interest, in this case: E', E'' and tan δ, see fig 3.13

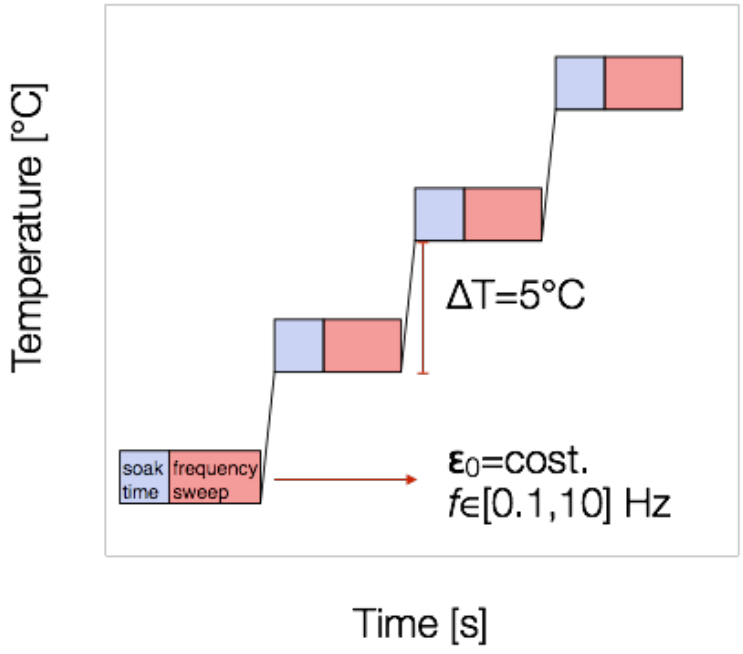

Figure 3.13: Schematic representation of temperature-frequency sweep tests

Also for these measurements two different procedures have been used:

- Procedure 1: $T \in [40,100]$ for adhesive B($r:h_1$), $T \in [40,110]$ for adhesive C. Temperature raised of 5°C between each step. Soak time of 5 minutes. $f \in [0.1,10]$ Hz. Air gas used as refrigerant.
- Procedure 2: $T \in [-15,40]$°C. Temperature raised of 5°C between each step. Soak time of 2 minutes. $f \in [0.1,10]$ Hz. Liquid N_2 used as refrigerant.

With the obtained data, E' and tan δ mastercurves are built through the application of the time-temperature superposition principle, TTS principle. In this way the material viscoelastic properties are analysed over a broader frequency range. This principle, concerning the time response of the materials with the temperature, is used to investigate the long-term response of viscoelastic materials[20] [21]. For polymer-composites materials the principle can be also applied[22], specially for temperatures in which the mechanical response of the non-polymeric phases is unaffected. In the case of Hybrix™ material a complication regarding the applicability of the mentioned principle may be due to the presence of two different polymeric phases within the core, although, as showed from the temperature ramp analysis, the nylon fibres don't seem to be detected. A deeper analysis on the principle validity and on the possible complexity of the polymeric core investigated will be given in paragraph 3.8. First a brief introduction about material damping properties is presented in the next paragraph

3.7 Damping properties of materials

The damping properties of a material represent simply its ability to dissipate energy during dynamic deformation. When it comes to sounds absorption properties, the sounds waves penetrating within a structure can be damped in a similar way as mechanical vibrations. Hence the ability of a material to absorb the sound can be also described by its loss factor, or tan δ [16].

Depending on the damping performance materials can be classified as high damping or low damping materials. The first find applications where the noise control, through reduced structures vibration, is crucial. Low damping materials instead are used when the sounds wave propagation is desired. Metallic materials, and metal matrix composites, shows generally low damping properties[23]. However, the possibilities opened up by polymer-metal composites, and lightweight materials, have generated an increased interest

in considering the damping performances as an important parameter during composite designing. Damping performance of a material are strongly influenced by the temperature, especially dealing with polymer or polymer-based composites[24]. Varying the temperature in a region close to the polymer T_g will lead to a change in the loss factor value of several order of magnitude. Table 3.3 shows this variation of the loss factor with the temperature, for different type of materials.

Material	Temperature range	Tan δ
Amorphous polymers	$T<T_g$	0,01 to 0,1
Amorphous polymers	$T> T_g$	0,1 to 1
Semi-crystalline polymers	$T_g<T<T_m$	0,1
Fiber-reinforced polymers	$T_g<T<T_m$	< 0,01
Metals	$T<T_m$	< 0,0001

Table 3.3: Materials loss factor variation with temperature, taken from[16]

From table 3.3 it's clear that the materials characterize by higher damping properties are amorphous polymers. A decrease in the loss factor is obtained passing to semi-crystalline polymers, or to fibres reinforced composite with polymeric matrix. But when compared to metal damping performances, even semicrystalline polymers or polymer-based composites could be considered high-damping materials.

3.8 Time-Temperature superposition principle

One of the main characterizing features of polymer materials its their viscoelastic behaviour, which means that their response to an external applied input, depending on the operating conditions, can range between the one of an elastic solid and a pure viscous liquid. Due to this characteristic polymer exhibit time dependent properties that are strongly influenced by the temperature. The temperature effect is a simple modification of the characteristic time response of the polymer. The reason behind this effect is found on the different amount of free volume, at different temperatures. High temperatures increase

the polymer free volume leading to an easier and faster mobility of the polymeric chains. Low temperatures instead decrease the amount of free volume slowing down the chain movement[16]. For example, when measuring the relaxation modulus of a generic polymer at different temperatures, the shape of the obtained curves remain almost the same. The main exception is that they would appear horizontally shifted with respect to a generic curve at a certain temperature, taken as a reference.

The time-temperature equivalence can be then used to shorten the experimental time window, especially in case of time-consuming test, and to increase in the same time the time scale of the observed phenomenon. Measurements made over a narrow range of time but over a wide range of temperatures, are assumed to be equivalent to measurements performed at one temperature but over a wide time scale[25]. A schematic illustration of the phenomenon just described is provided in figure 3.14.

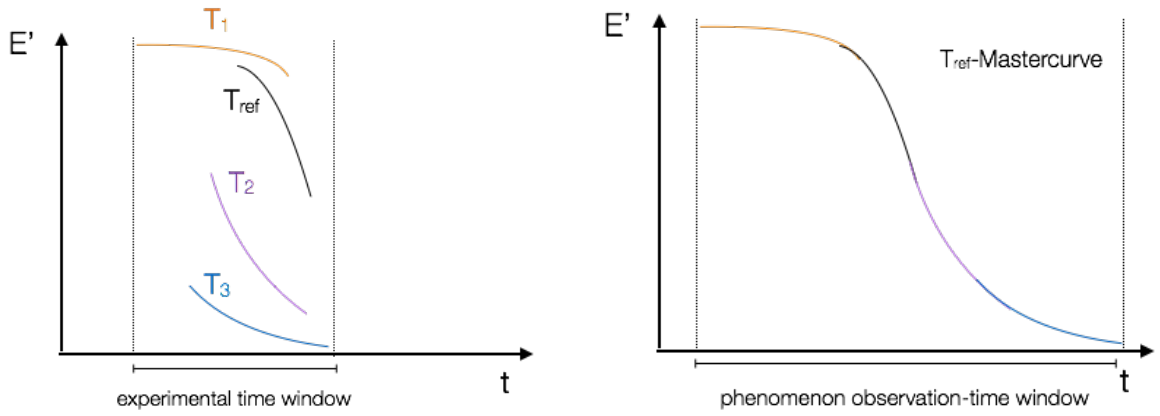

Figure 3.14: Storage modulus measurements at different temperatures on the left, storage modulus mastercuve built applying the time temperature superposition principle on the right

The curves obtained from the measurements at different temperatures can be reduced to a single mastercuve at a reference temperature. The mastercuve is simply obtained by shifting all the data with respect to the selected reference temperature. This is the base of the so called time-temperature superposition principle.

The amount the curves are shifted is represented by a temperature-dependent shift factor α_T, which can be defined as follow:

$$log\alpha_T = log\frac{t}{t_{T_{ref}}} \qquad \text{(eq. 3.8)}$$

$$log\alpha_T = -\frac{C_1(T - T_{ref})}{C_2 + (T - T_{ref})} \quad \text{(eq. 3.9)}$$

where t is the time response of the polymer at the temperature T at which we are evaluating the shift factor, while the t_{Tref} is the one at the reference temperature. Equation 3.8 represents the Williams, Landel and Ferry, WLF, equation, in which C_1 and C_2 are two empirical constants, which change depending on the different material analysed. Choosing the polymer T_g as a reference temperature average values of C_1 and C_2 were estimated to be respectively 17,44 and 51,6, and to fit for a large number of polymers[26].

$$log\alpha_T = -\frac{17{,}44 * (T - T_{ref})}{51{,}6 + T - T_{ref}} \quad \text{(eq 3.10)}$$

The same considerations of the time-temperature superposition principle can be applied for the frequency, being intrinsically dependent on the time. In this case the low temperature tests will describe the polymer response to high frequencies in the obtained mastercurve, while the high temperature tests the low frequencies response:

$$log\alpha_T = log\frac{\omega_{T_{ref}}}{\omega} \quad \text{(eq. 3.11)}$$

Here the advantage is obviously a possible investigation over a broad frequency range, reaching also frequencies that would otherwise be very difficult to investigate experimentally.

A material to which the time-temperature superposition principle is applicable, in a sense that a proper-fitting mastercurve can be obtained, is defined as being thermorheologically simple[27]. Thermorheological simplicity means also that the time response of all material's viscoelastic properties is characterized by the same temperature dependence. This implies that the different viscoelastic function investigated can be shifted by the same shift factor, α_T.

3.9 Temperature-frequency: experimental results and discussion

The first tests were performed according to procedure 1, on both adhesive B(r:h_1) and C samples. The two samples are characterized by different facing material. As specified in paragraph 3.7 the damping properties of metal materials are several orders of magnitude lower when it comes to comparing it with polymer. Following this consideration the damping properties here measured are assumed to be related only to Hybrix^{TM} polymeric core, and in particular to the adhesive material. The curves in fig 3.15 shows the variation of the storage modulus, E', and of the loss factor, tanδ, with frequency and temperature. In order to build the composite mastercurve, an horizontal shifting for each obtained curve was performed, choosing as a reference temperature the adhesives T_g, i.e. 50°C for adhesive B(r:h_1) and 70°C for adhesive C. The shifting was done through the RSI Orchestrator software supplied with the DMA Rheometrics RSA II. Using the TTS application, each curve is shifted according to a single shift factor, α_T, until an optimal overlapping of the curves is reached. The two adhesives mastercurves and their shift factor variation with temperature, according to the WLF equation, are showed in fig 3.16.

Comparing the results of the two different adhesives samples it appears how, beside the last curve of the storage modulus, a more accurate superposition occurs for the sample characterized with the adhesive C. For the adhesive B sample instead a limitation of the principle reliability is denoted, mostly for the storage modulus mastercurve. As a matter of fact, the curves describing the low frequency behaviour don't show a proper fitting.

If the adhesive B(r:h_1) curves are instead shifted (by manual procedure) using different shift factors for the two viscoelastic functions the mastercuvers obtained show an optimal fitting, see figure 3.17. The shift factor for the storage modulus seems also to fit in good agreement with the generalized WLF equation, expressed in eq. 3.9.

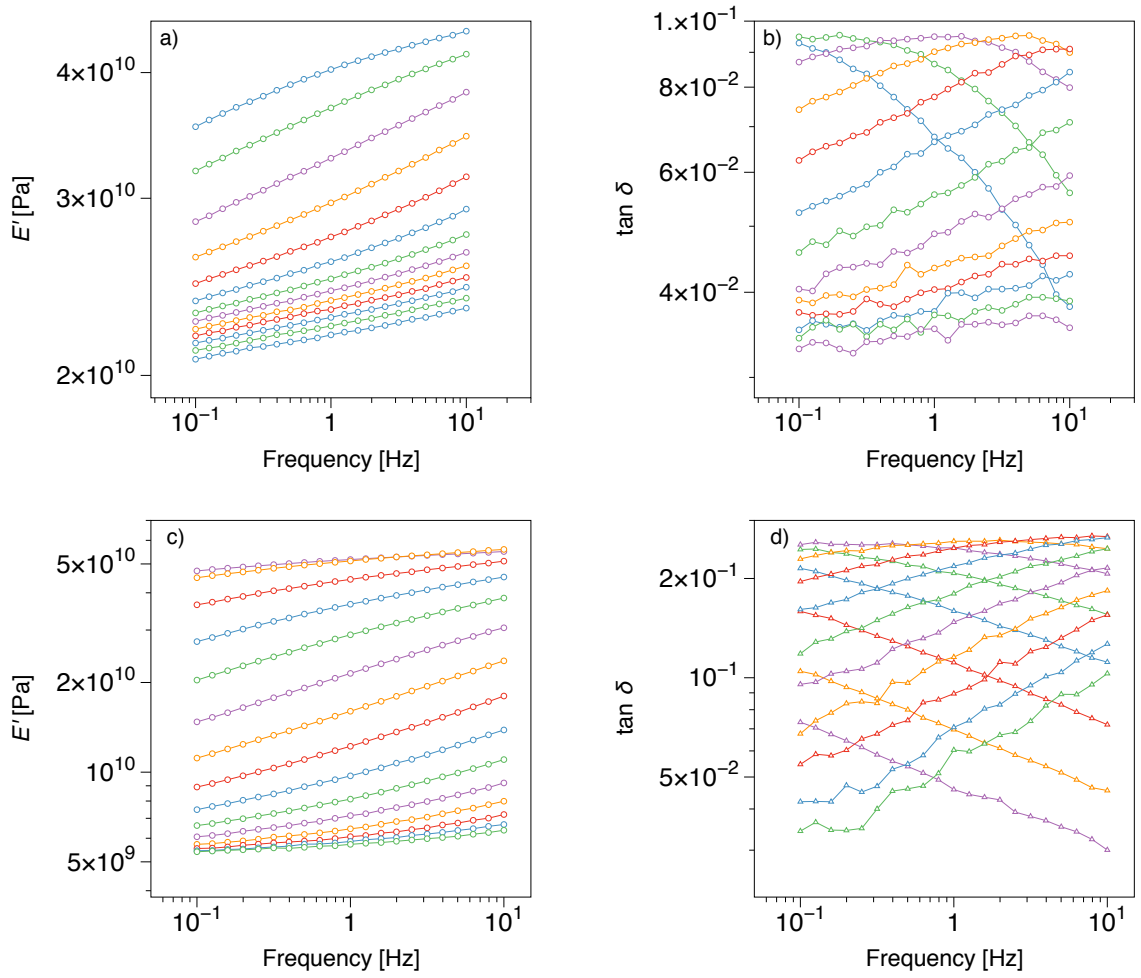

Figure 3.15: Storage modulus and tan δ temperature-frequency sweep for adhesive B(r:h_1) (a-b), and for adhesive C (c-d)

Using different shift factors would denote a different dependence of the viscoelastic properties with respect of the temperature, and thus a thermorhelogical complexity of the investigated material[28]. The different thermorheological complexity of the two adhesives could be explained by considering their different nature. Adhesive B is indeed characterized by two different components, a resin and a hardener needed for the activation of the crosslinking process. The adhesive C instead is a single component epoxy, whose crosslinking is simply thermally induced.

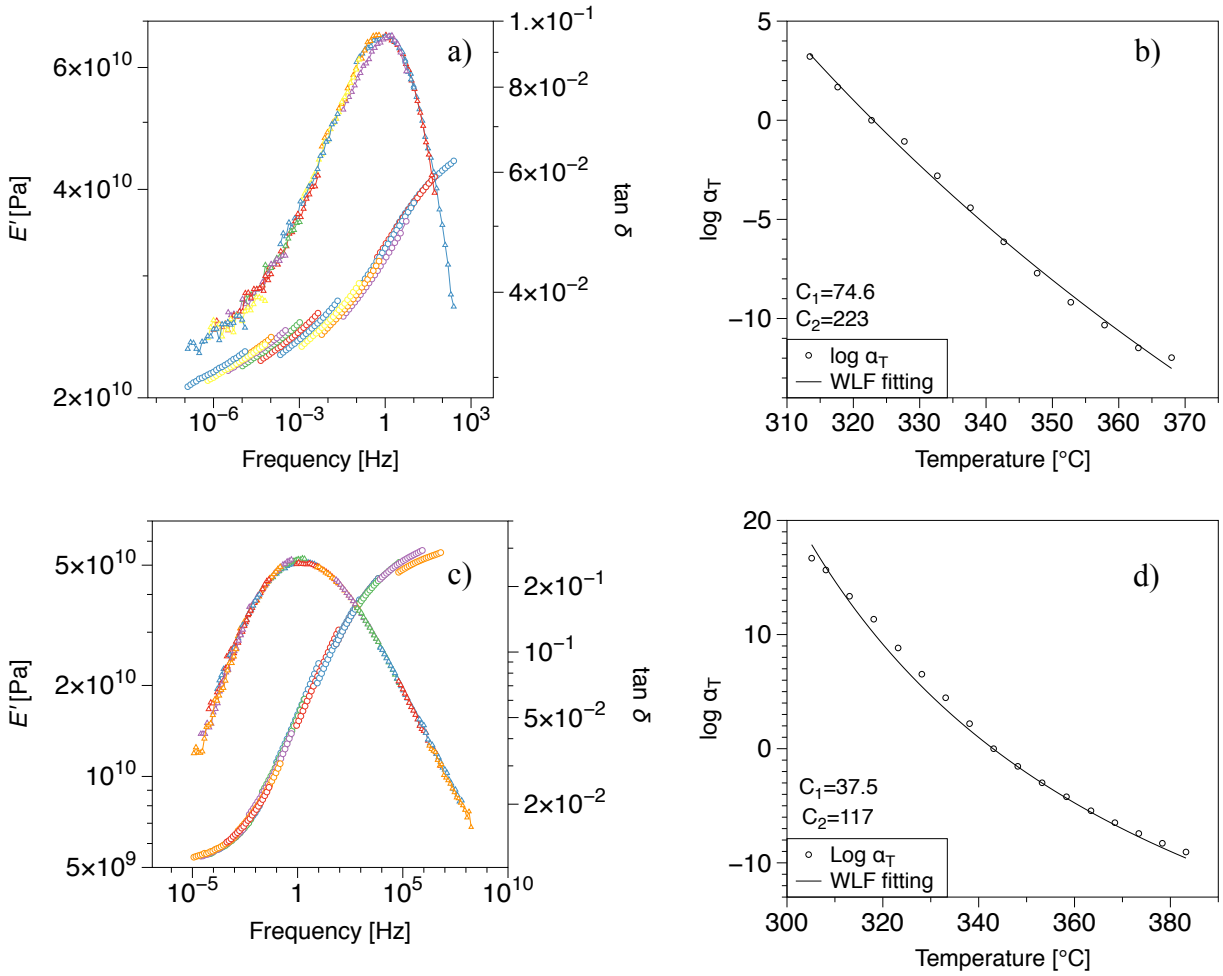

Figure 3.16: Mastercuves of storage modulus and tan δ at 50°C for adhesive B(r:h_1) (a) and variation of the shift factor with temperature (b). Mastercurve of storage modulus and tan δ at 70°C for adhesive C (c) and variation of the shift factor with temperature (d)

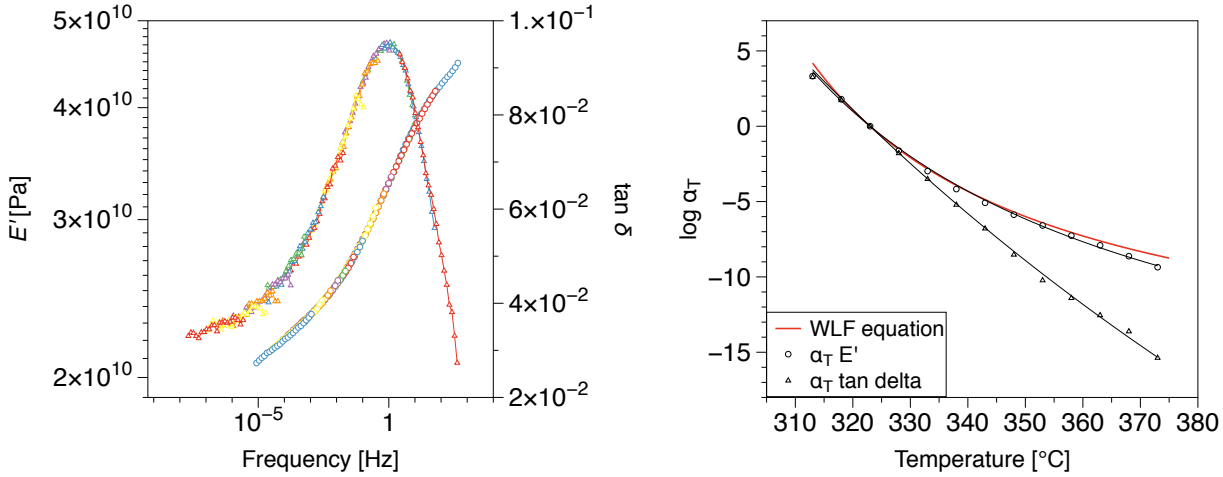

Figure 3.17: Mastercurve of storage modulus and tan δ of adhesive B(r:h_1) at 50°C obtained with two different shift factors

As an estimation of the possibility to perform correctly the time-temperature superposition, or to investigate the thermal complexity of polymeric materials, some studies refers to Wicket's plot[29]. These curves are obtained from the data acquired with the temperature-frequency sweeps, plotting the loss factor with respect of the storage modulus. All the values, measured at different temperatures, should fit in a unique and symmetric curve.

Following this procedure for the two tested adhesives the plots showed in figure 3.18 are obtained. It appears clearly that the wicket plot for the adhesive C fits much better than the one of adhesive B, strengthening the hypothesis of the different thermal complexity of the two adhesives, within the investigated temperature range.

In order to obtain the damping performance of the Hybrix^{TM} at high frequency but at lower temperature than their T_g, another temperature-frequency sweep for an adhesive C sample was performed, this time according to procedure 2. The obtained mastercurve at 20°C of the adhesive C is showed in figure 3.19. As can be seen, at low temperatures the obtained curves don't show the same smooth fitting depicted from the mastercuve at 70°C. Especially for the curve of the loss factor.

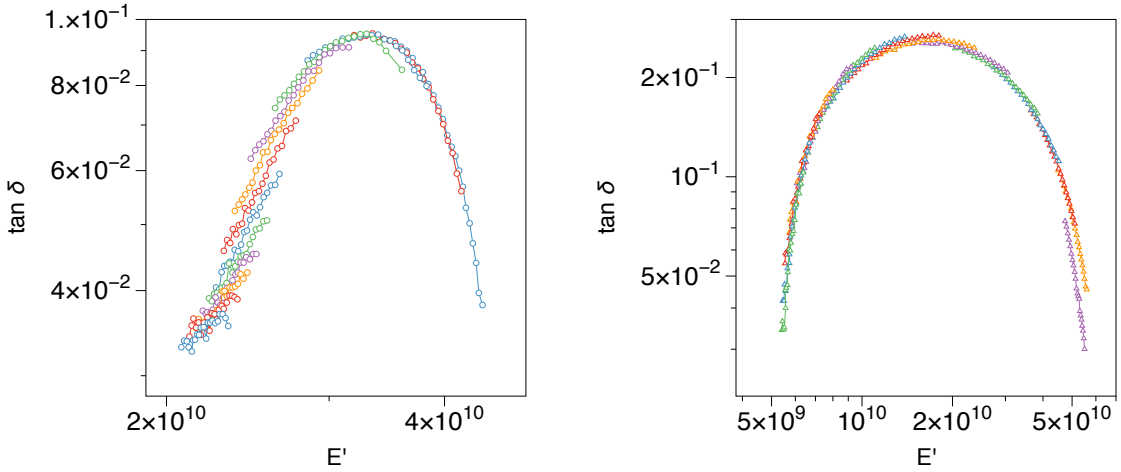

Figure 3.18: Wicket plots showing tan δ vs. E' for adhesive B(r:h_1) on the left, for adhesive C on the right

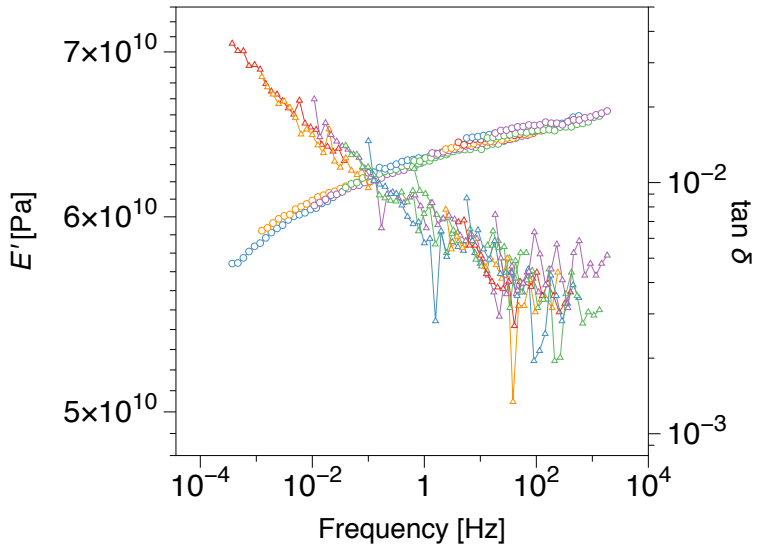

Figure 3.19: Mastercurve of storage modulus and tan δ at 20°C for adhesive C

Independently from the accuracy of the obtained mastercurve at this temperature, it is still possible to denote a strong reduction of the loss factor from the values measured at 70°C. In order to properly exploit the damping performance of Hybrix^{TM} application temperature close to the adhesive T_g are then recommended.

3.10 Temperature-frequency sweep: conclusion summary

From the tanδ mastercurves of figure 3.16 a) and c), an evaluation of the damping performance of Hybrix^{TM} up to 200 Hz, for both adhesives is presented in table 3.4:

Adhesive type	Evaluation temperature	tan δ variation with frequency [1-200 Hz]
B(r:h_1)	50°C	0,1 to 0,04
C	70°C	0,25 to 0,18

Table 3.4: Hybrix^{TM} damping properties variation with frequency

From the reported values it appear that adhesive C is characterized by higher damping properties. Figure 3.20 shows a comparison between the loss factor values of Hybrix^{TM} SPC sample with other common values measured for other type of materials, taken from table 3.1. Here is possible to mark the higher performance between the tested sandwich structure and another class of composite material: i.e. fibre reinforced composites, FRC.

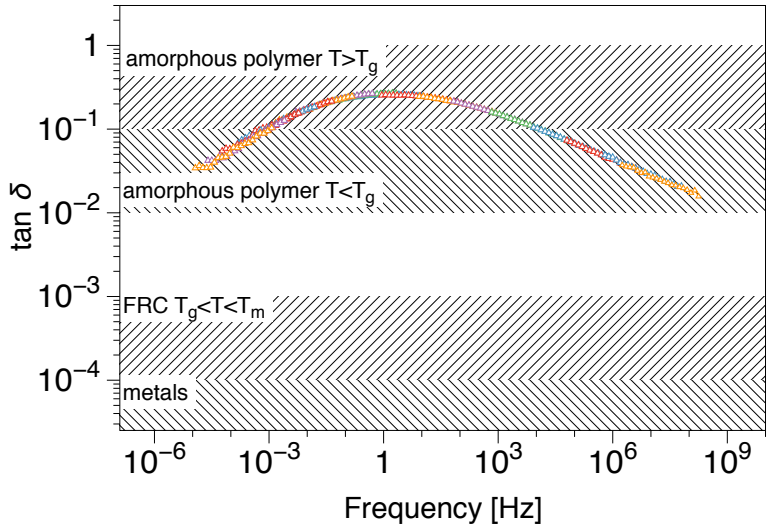

Figure 3.20: SPC loss factor compared with loss factor of other class of materials

As it appears also from figure 3.20 the loss factor measured for the sample with adhesive C is comparable to loss factor values measured for amorphous polymers, commonly used in designing materials for damping applications[30].

4 Bending stiffness of sandwich materials

In this chapter the experimental procedure for the evaluation of the Hybrix^{TM} bending stiffness and its core shear modulus according to the first-order shear analysis is presented. An introduction on the bending stiffness characteristics for sandwich composite materials and the theoretical assumption behind the first-order shear analysis will be discussed first.

4.1 Bending stiffness for sandwich composites

The main feature of the Hybrix^{TM} sandwich is its high bending stiffness, combined with the weight reduction gained in comparison with solid metals, such as stainless steel and aluminium. According to the classical beam theory, the bending stiffness can be defined as the proportionality between an applied moment M and the resulting beam curvature k. For an homogeneous material this is simply obtained by the product of its elastic modulus E and the moment of inertia of the beam cross section I. Assuming a rectangular cross section for the beam, and a central load applied, this can be expressed by the following equations.

$$M = EIk \qquad \text{(eq. 4.1)}$$

$$D = EI = \frac{Ebh^3}{12} \qquad \text{(eq. 4.2)}$$

$$I = \int_0^h y^2 dA \qquad \text{(eq. 4.2)}$$

in which b and h represent respectively the width and the thickness of the structure. For sandwich materials whose application doesn't require elevated mechanical performance, and thus complex design analysis, a simplified but common approach is to apply the same classical beam theory assumptions. The structural design of sandwich materials can then follow the traditional design methods applied for loaded panels[31]. In this case the main difference with respect to a homogeneous solid beam, is that the different contribution to overall flexural rigidity of the different phases forming the element has to be considered. The overall bending stiffness EI of a sandwich beam can be then expressed, through the parallel axis theorem, as:

$$D = E_c I_c + 2E_f I_f \qquad \text{(eq. 4.4)}$$

where E_c stands for the modulus of the core, while E_f for the modulus of the facing material. Having so the sandwich bending stiffness simply given by the sum of the rigidities of the core and of the two facing. The two different momenta of inertia can be expressed as:

$$I_c = \frac{bh_c^3}{12} \qquad \text{(eq. 4.5)}$$

$$I_f = \frac{bh_f^3}{12} + \frac{bh_f d^2}{4} \qquad \text{(eq. 4.6)}$$

leading then to the more common expression of the bending stiffness per unit width[8]:

$$\frac{D}{b} = \frac{E_c h_c^3}{12} + \frac{E_f h_f^3}{6} + \frac{E_f h_f d^2}{2} \qquad \text{(eq. 4.7)}$$

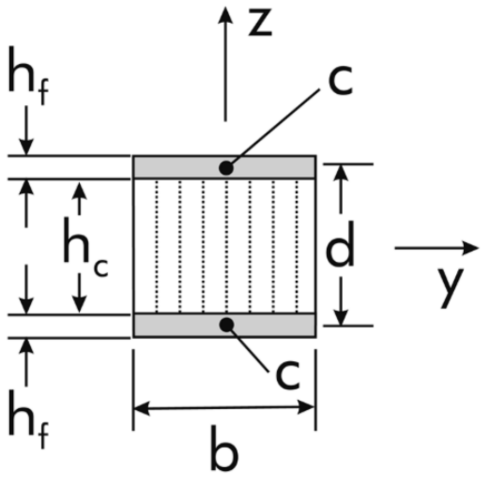

Figure 4.1: Sandwich composite cross section

in which h_c and h_f stands respectively for the thickness of the core and the one facing, while d as the distance between facing's centroids, as it can be seen from figure 4.1. If we define E_b as the effective flexural modulus of the sandwich beam, it's possible to express the bending stiffness also as:

$$D = \frac{E_b bh^3}{12} \qquad \text{(eq. 4.8)}$$

it's possible to get an useful expression for E_b, after some algebraic manipulation of eq. 4.7[31]:

$$E_b = E_c \nu^3 + E_f(1 - \nu^3) \qquad \text{(eq 4.9)}$$

with ν being the core/sandwich thickness parameter:

$$\nu = {h_c}/{h_f} \qquad \text{(eq 4.10)}$$

where h stands for the total sandwich thickness. It's easy to understand how eq. 4.8 and 4.9 represent powerful instruments in designing sandwich materials, in order to have a theoretical estimation of the sandwich flexural stiffness E_b and then also of its bending stiffness D, once the facing and core materials properties are known. The same approach can be extended for the evaluation of other useful sandwich characteristics as the ultimate bending momentum M_u, or the least-weight sandwich construction for a given bending stiffness. In order for this analysis to be valid, we assume that the classical bending theory may be applied to our sandwich structure. Hence the cross-section, plane and perpendicular to the neutral axis of the unloaded beam, remain so after the deformation. A composite sandwich material can fall within this assumption if characterized by a core stiff in shear, in order to have negligible shear deformation in bending, and a narrow beam width in order to consider negligible transverse stresses parallel to the facing. We can assume a core to be stiff in shear if[31]:

$$\frac{D}{l^2 Q} < 0.01 \qquad \text{(eq. 4.11)}$$

where l represents the beam length, and D and Q the bending and shear stiffness. This condition is obtained considering the deflection of a beam, at the point of load application, simply supported at the ends in a three-point bending test, assuming negligible the contribution to the deflection given by shear. From the above eq. it's then possible to obtain a critical beam length l^* above which the shear effects are small:

$$l^* = 10\left(\frac{D}{Q}\right)^{1/2} \quad \text{(eq. 4.12)}$$

As previously stated, this theoretical approach for the evaluation of sandwich materials characteristics, as its flexural modulus and consequentially its bending stiffness, requires the knowledge of the sandwich components properties, E_f and E_c. For sandwich materials characterized by a complex core design, like for Hybrix^{TM}, this represents a limitation, due to the difficulty to test and measure the core properties separately from the metal facing. In order to offset this limitation, another approach has been used which enables the determination of the sandwich bending stiffness D and the core shear stiffness Q, through three-point bending tests following the first-order shear deformation analysis. This analysis will be discussed in the paragraph 4.3; first the thin-face approximation for sandwich material will be discussed.

4.2 Thin face approximation

It is common to express the bending stiffness for unit width of eq. 4.7 simplified as follow:

$$D = E_f h_f d^2 \left[\frac{h_c^3}{12 h_f d^2}\left(\frac{E_c}{E_f}\right) + \frac{1}{6}\left(\frac{h_f}{d}\right)^2 + \frac{1}{2}\right] \quad \text{(eq. 4.13)}$$

Analysing now the single components of equation 4.13 a simplified expression of the bending stiffness can be obtained which is valid for some sandwich configurations. The first term within the brackets is generally really small, considering the small core-to-face modulus ratio, generally $E_c/E_f \propto 10^{-3}$. The second term gives a strong contribution only in the case of thick faces, while the most common used sandwich structures are characterized by thin strong facing bonded to a thick lightweight material. Hence, usually a limiting core/face thickness ratio is established above which the contribution to the bending stiffness given by the first two terms is below 1%[8]:

$$\frac{h_c}{h_f} \geq 5.35 \quad \text{(eq. 4.14)}$$

If this inequality is satisfied, the facing may be considered thin and the overall bending stiffness can be computed by the equation eq. 4.15, neglecting the contribution of the first two terms:

$$D = \frac{E_f h_f d^2}{2} \qquad \text{(eq. 4.15)}$$

with this simplified expression we can furthermore denote the main factors which lead to high values of the bending stiffness: face sheets with high modulus, E_f, and a large distance between the facing's centroids, d. However it may seems beneficial also to have high facing thickness to achieve high bending performances, this will not be optimal regarding the weight saving issue. Considering then both factors the most convenient sandwich design will be characterized by thin and high modulus facing, bonded to thick low density core. A list with the most common material used as sandwich facing and their mechanical properties is reported in table 4.1

Material	Density, g/cm^3	Young's modulus, GPa	Shear modulus, GPa
Stainless steel AISI 304L	7,9	193-200	78
Aluminium 5083 H22	2,6	71	27
Glass/EP	2	26,6	4,63
Carbon/EP	1,63	59,5	4,96

Table 4.1: Common facing material properties, taken from[8]

The alloy for the stainless steel and for the aluminium reported in table 4.1 is the type used by Lamera, AB for the production of the Hybrix^{TM} product. The other two composite facing stands for epoxy matrix reinforced respectively with glass fibre (Glass/EP) and carbon fibre (Carbon/EP).

4.3 First-order shear analysis of sandwich beams with three-point flexure loading

The main difference in the assumptions between the first-order shear analysis in comparison with the classic beam theory, is that the first-order theory assumes the cross-section of the core, after deformation, to remain plane, but it may be not anymore perpendicular to the deformed beam neutral axis, as shown in fig 4.2

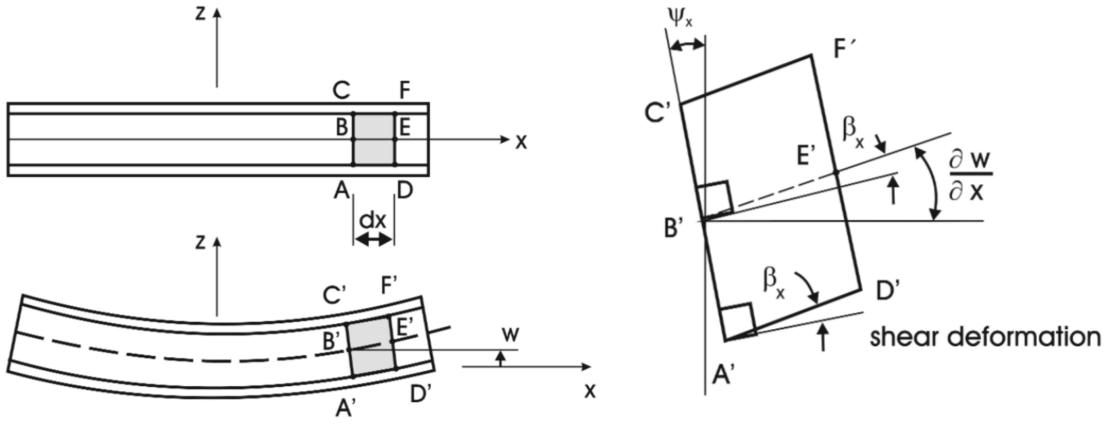

Figure 4.2: Deformation of the core in the x-z plane

The other assumptions on which this theory is based on are the following[8]:

- Face sheets thin compared to the core, $h_f << h_c$, and a plane state of stress, $\sigma_z=0$
- In-plane stresses in the core are negligible
- Out-of-plane displacement w is independent of the z coordinate, $\varepsilon_z = {}^{\partial w}/_{\partial z} = 0$
- The in-plane displacements in the core are linear in the thickness coordinate z

The differential equation governing the bending of the beam is described in eq. 4.16, in which ψ_x stands for the rotation of the cross-section originally perpendicular to the x axis, G_{xz} for the core shear modulus, and M_x for the applied bending momentum. All the equilibrium equations that precede this and which follow from first-order theory assumptions will not be reported here.

$$\frac{dw}{dx} = -\psi_x + \frac{1}{h_c G_{xz}} \frac{dM_x}{dx} \qquad \text{(eq. 4.16)}$$

Under a three-point bending load with a span length of L, as the one showed in fig 4.3, we can express the bending moment as:

$$M_x = \frac{-Px}{2b} \qquad 0 \le x \le \frac{L}{2} \tag{eq. 4.17}$$

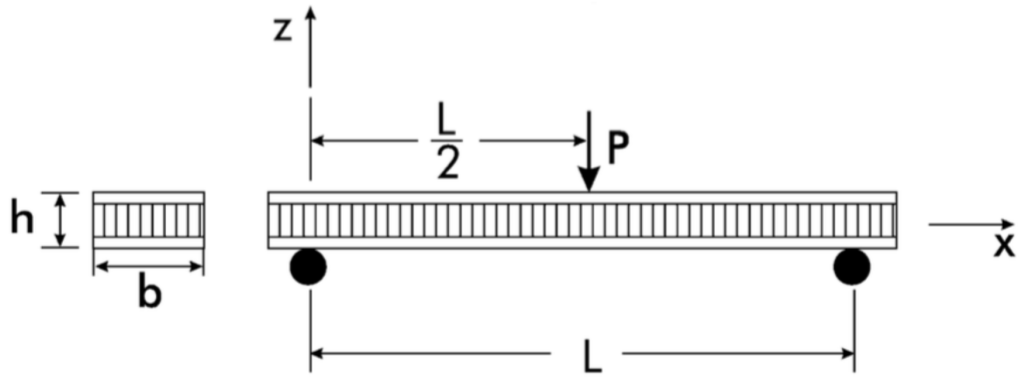

Figure 4.3: Sandwich beam under three-point flexural load

solving the differential equation 4.16 at the point of load application, which is the point characterized by the highest deflection, this yields to:

$$\delta = \frac{PL^3}{48bD} + \frac{PL}{4h_c bG_{xz}} \tag{eq. 4.18a}$$

If we express now eq. 4.18a as follows

$$\delta = \frac{PL^3}{48Db}\left[1 + \frac{12D}{L^2 h_c bG_{xz}}\right] \tag{eq. 4.18b}$$

it's possible to better understand the origin for a stiff core condition, eq. 4.11, which allows to neglect the contribution given from the shear ($D_x/(L^2 h_c b G_{xz})$), yielding to the definition of the bending stiffness through eq. 4.7:

$$D = \frac{PL^3}{48b\delta} = \frac{E_b bh^3}{12} \tag{eq. 4.19}$$

$$E_b = \frac{L^3}{4bh^3}\frac{P}{\delta} \tag{eq. 4.20}$$

Starting from equation 4.18a, a useful method for the determination of the shear and bending stiffness of sandwich beams, from tests conducted in the linear-elastic regime and at small loads, can be obtained. The same method has been applied for sandwich materials characterized by complex core configuration: polymeric foam with through thickness reinforcing fibres[32].

The compliance, C, of the three-point bending tested specimen can obtained and expressed with respect to the loading span, as proposed by Allen (1969), as follows:

$$C = \frac{\delta}{P} = \frac{L^3}{48bD} + \frac{L}{4bh_c G_{xz}} \quad \text{(eq. 4.21a)}$$

$$\frac{C}{L} = \frac{L^2}{48bD} + \frac{1}{4bh_c G_{xz}} \quad \text{(eq. 4.21b)}$$

$$\frac{C}{L^3} = \frac{1}{4bh_c G_{xz}} \frac{1}{L^2} + \frac{1}{48bD} \quad \text{(eq. 4.21c)}$$

Hence if then compliance is determined over a range of span lengths, and the results plotted in linear graphs, C/L vs. L, and C/L^3 vs. $1/L^2$, as showed in figure 4.4, it's possible to obtain a graphical evaluation of the bending stiffness and the core shear modulus from the slopes, m_1 and m_2, simply from the following equations:

$$m_1 = \frac{1}{48bD} \quad \text{(eq. 4.22)}$$

$$m_2 = \frac{1}{4bh_c G_{xz}} \quad \text{(eq. 4.23)}$$

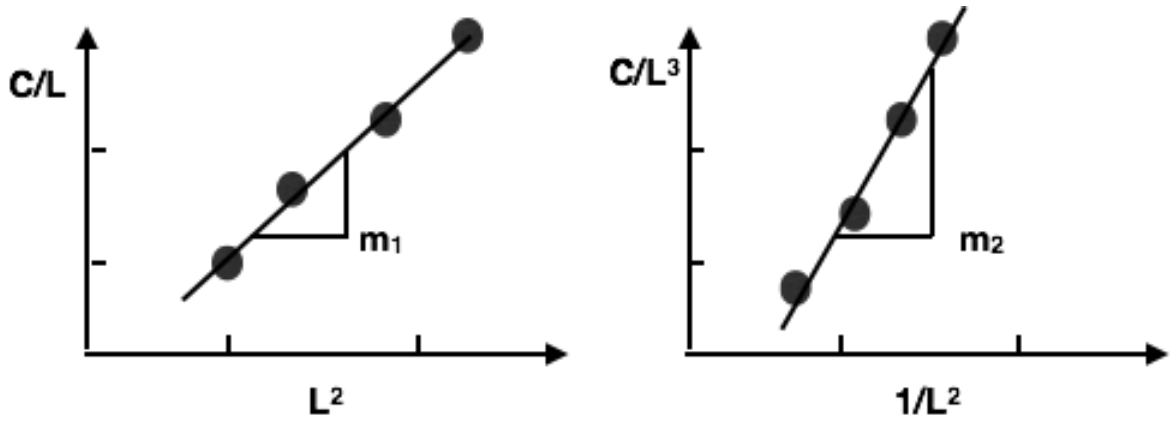

Figure 4.4: Graphical evaluation of bending stiffness and core shear stiffness of sandwich materials

In the next paragraph the experimental settings and the obtained results are discussed.

4.4 Experimental procedure and results discussion

For the measurement of the bending stiffness of Hybrix^{TM} material the following procedure was adopted. Three of the available Hybrix^{TM} sandwhich configurations, falling within the thin-face approximation, were tested according to the procedure described in the first-order shear analysis. To check method reliability, the measured bending stiffnesses were then compared to the one expected from the thin-face approximation. The tested materials specifications are listed in table 4.2

Hybrix type	h_{tot} (mm)	h_f (mm)	h_c (mm)	h_c/h_f
SPB(r:h_1)	1,65	0,15	1,35	9
SPB(r:h_3)	1,55	0,15	1,25	8,33
SPC	1,4	0,15	1,1	7,33

Table 4.2: Specification of tested samples

The tests were performed with an Instrom 5500R, with a maximum load of 100 KN, setting the operating conditions and the sample geometry as reported in the ASTM 393/C393M and ASTM D7250 standards for sandwich beam properties by beam flexure. For sandwich materials characterized by unknown facing modulus the standards state the need to use two loading configurations to obtain the overall bending stiffness of the

sandwich, and this procedure as been followed also in some other studies[33]. If the modulus of the facing material is known one loading configuration can be used.

The sample's geometry was the same for all the tested specimen, 150 mm length and 25 mm width. The tests were performed with a 3-point mid-span loading fixture, as can be seen in fig 4.5.

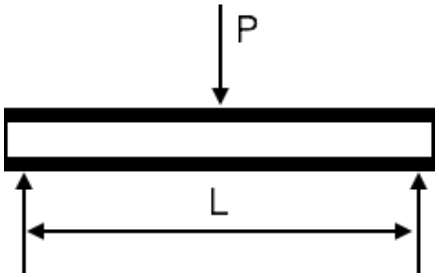

Figure 4.5: Sandwich beam undear 3-point mid-span flexural load (P)

The loading bars were 15 mm diameters steel cylinders, while the speed for cross-head displacement, considering the low thickness of the tested samples, was set at 1 mm/min.

Four different loading spans were selected for testing the specimens, L=100 mm, L=90 mm, L=80 mm and L=70 mm. For each Hybrix^{TM} type, listed in table 4.2, four samples were tested. The first for each was tested with the highest span length until a clear elastic region was obtained. The other tests, varying the four different span lengths for each sample, were then performed and stopped at a selected limiting force within the elastic region. A limit load of 30 N was chosen for all the tests. The curves of load vs. deflection of the first samples for the three different Hybrix configurations, and an example of the one obtained for different span lengths are shown in figure 4.6.

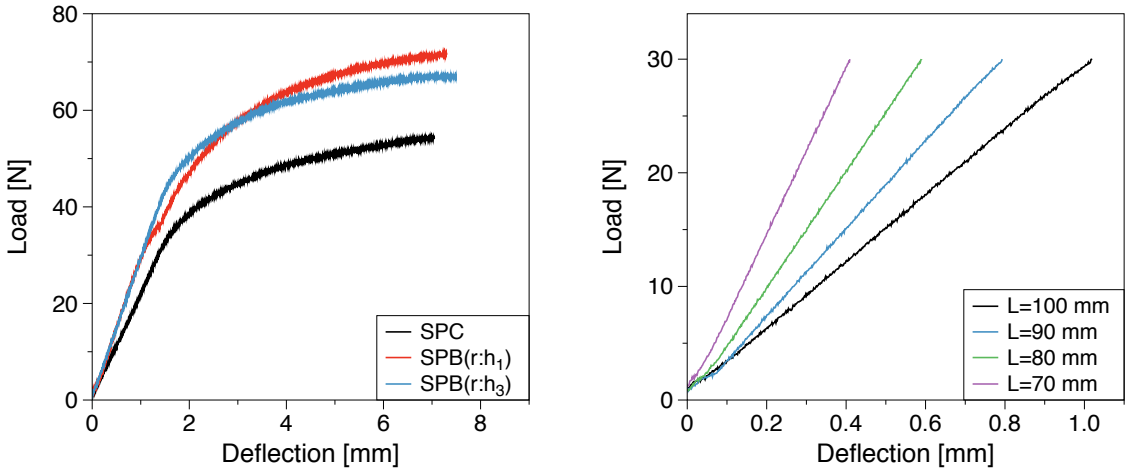

Figure 4.6: Load vs. deflection curves for L=100 mm for every first Hybrix^{TM} sample on the left, load vs. deflection curve with different span length up to 30 N on the right

From the data obtained, plots of the compliance vs L and $1/L^2$ were obtained, see fig 4.7, and the average flexural bending stiffness and shear stiffness was calculated and listed in table 4.3

Sample	D thin-face approximation	$D_x=1/48bm_1$	$G_{xz}=1/4bh_cm_2$
SPB (r:h_1)	32,5-33,75 Nm	28,82 Nm	138 MPa
SPB(r:h_3)	28,4-29,4 Nm	30,13 Nm	109 MPa
SPC	22,6-23,4 Nm	20,18 Nm	224 MPa

Table 4.3: Obtained values of bending stiffness and core shear modulus

The experimental measured values are in good agreement with those expected from the thin-face approximation, whose value was derived from equation 4.15 using as E_f the values listed in table 4.1 for stainless steel AISI 304.

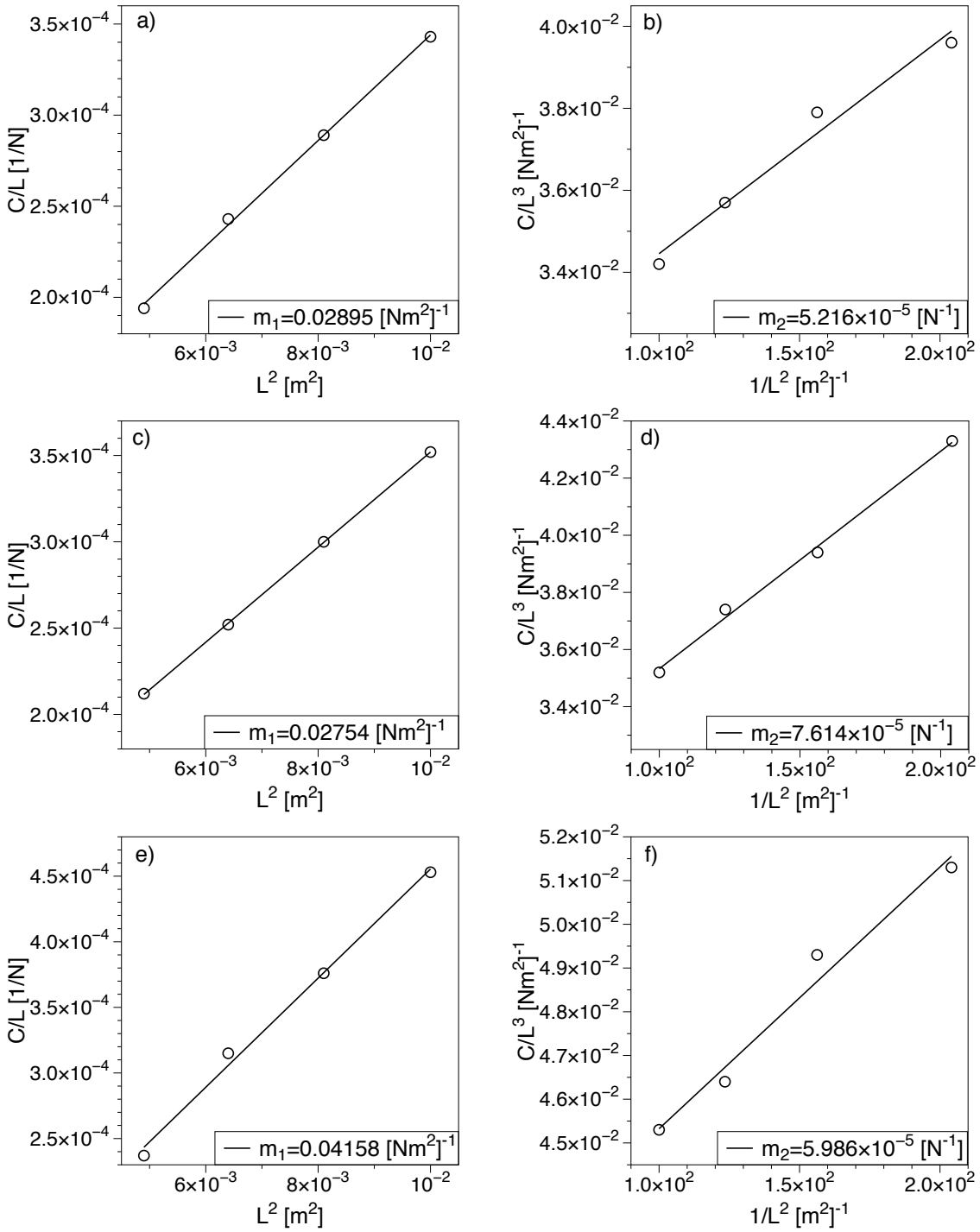

Figure 4.7: Graphical evaluation of bending stiffness and core shear stiffness of Hybrix^{TM} SPB(r:h_1) (a-b), SPB(r:h_3) (c-d), SPC (e-f)

The relative error between the values ranges from 5-10%. From the evaluation of the Hybrix^{TM} shear core modulus interesting information can be pointed out. The values obtained are higher than common shear modulus values of polymeric cores, see table 4.2. The reasoning for this can be provided by Hybrix^{TM} innovative core design, characterized

by the nylon fibres, present in high amount (~200 g/m^2), which act as a reinforcement in the through-thickness direction of the sandwich material.

Another interesting aspect comes from the core shear modulus value for the sample with the adhesive C. It appears from the measurements to be the one with the highest shear rigidity. This result can further explain the outcomes of the temperature ramp tests. As a matter of fact the Hybrix^{TM} samples characterized with adhesive C were the only one not affected by delamination. This would prove a better resistance of the core to shear stresses, and a better transfer of the shear loads from the core to the facing, even at room temperature.

5 Nickel pulse electrodeposition

In this chapter the pulse-electrodeposition of a thin nickel layer on the stainless steel metal facing of Hybrix^{TM} is described. First, an overview about electrodeposition of nanocrystalline metal structures is provided, afterwards the properties of such materials and the previous work done in this field is presented. The obtained nickel film is characterized with EBSD and TEM analysis in order to evaluate its microstructural characteristics: i.e. grain size, grain size distribution, and crystallographic orientation. Nanoindentation tests are performed to evaluate the Vickers hardness.

5.1 Electrodeposition of nanocrystalline metals

Since their first introduction nanocrystalline materials have been of great interest and produced by numerous synthesis techniques. Between all the different processing techniques, five distinct groups can be distinguished: vapour phase processing, liquid-phase processing, solid-state processing, chemical synthesis and finally electrochemical synthesis. The distinguishing features of electrochemical synthesis with respect to the others mentioned is that it involves an interface between the substrate and the deposited species, at which a charge transfer occurs. Within electrochemical synthesis we can further distinguish between electrodeposition and electroless deposition. In the first, the reaction between the depositing species and the substrate is driven through the application of an external power supply (direct current or pulsed current), while in electroless deposition the addition of a reducing agent to the base metal electrolyte ensures the deposition process[34].

Recently, electrodeposition has proven to be an effective method for the production of nanocrystalline material[35] The benefit of this technique is the possibility to ensure a good control of the size of the obtained grains and of their crystallographic orientation, which then will reflect on the final material properties. As a matter of fact, these material characteristics are strongly influenced by the electrodeposition parameters applied, which control the deposition mechanism. Electrocrystallization occurs either by the build-up of previous existing crystals, i.e. by grain growth, or by the formation of new ones in form of nucleation[36]. The two key mechanisms that have been identified as the determining steps for nanocrystal formation are the charge transfer at the electrode surface, and the surface diffusion of the deposited species on the growing crystal structure. The microstructure

evolution in terms of grain size and grain orientation is indeed obtained with the surface diffusion inhibition through adsorption of foreign species on the growing surface of the electrodeposited material. The charge transfer, expressed as the current density applied, determines which mechanism is predominant between grain growth and new nuclei formation. The first is favoured at low current densities and high diffusion rates while high current and low diffusion rates yield new nuclei formation[34]. However, it is difficult to generalize the effect of these two parameters on the final structure without considering the other electrodeposition variables. In fact, different results have been obtained (i.e. smaller grains at low current densities) with different combinations of the electroplating parameters. A more in depth discussion of the other parameters and of their influence on the final crystal structure will be provided in paragraph 5.3.

5.2 Nanostructured material properties

Over the past years, electrodeposited nanomaterials have been studied extensively, and many of their physical, chemical and mechanical properties have been investigated as a function of grain size[34]. It must be said that for some of the properties, mostly mechanical properties, the understanding of the mechanisms regarding nanocrystals is still far from complete. Not all the material properties are however affected by the grain size, and for this characteristic are often classified as having a weak grain size dependence or, in the opposite case, as having a strong grain size dependence.

In the first group we find: saturation magnetization, heat capacity, thermal expansion, and Young's modulus. In the other group instead: Vickers hardness, yield strength, tensile elongation and wear rate. In this paragraph only the properties that can be of interest for this project will be described (Young's modulus, yield strength, hardness and tensile elongation), and will be referred always to nanocrystalline nickel since it's the material that will be used in this project.

In table 5.1, the grain size dependence of nickel's Young's modulus, yield strength, hardness and tensile elongation is shown. As can be seen, only the Young's modulus is not affected by the grain size, while all the other properties are strongly influenced. Nanocrystalline nickel with grain size around 10 nm has essentially the same Young's modulus of a conventional polycrystalline nickel.

Property	Conventional nickel	Nano-nickel (100nm)	Nano-nickel (10 nm)
Yield strength, MPa (25°C)	103	690	>900
Ultimate tensile strength, MPa (25°C)	403	1100	>2000
Tensile elongation, % (25°C)	50	>15	1
Modulus of elasticity, GPa (25°C)	207	214	204
Vickers hardness, Kg/mm^2	140	300	650

Table 5.1: Table extrapolated from A. Robertson et al., Nanostruct. Mat 12 (1999) 1035

It should be mentioned that values for Young's modulus reported for conventional electrodeposits can vary even for the same material when it was produced with different electrodeposition parameters[37]. Different reasons can be found for this fact: (i) difficulties in measuring elastic properties of thin coatings, (ii) not fully dense nanocrystalline structure, (iii) and possible different crystallographic texture. For the other mentioned mechanical properties the same problem can be incurred.

The properties that are affected the most from the reduction of the grain size to the nanoscale are clearly the hardness and the yield strength. The great increase in strength and hardness of nanocrystalline nickel, and more in general of metals, are the main factors attracting interest in this class of material, and thus in this project. The possibility to enhance properties of light-weight polymer based composites like Hybrix™ with a thin layer of a nanocrystalline metal represent an innovative field with a broad range of new possible applications for this class of materials. This considerable increase in both hardness and yield strength with decreasing grains size follows the Hall-Petch behaviour described for the yield strength by the following equation[38]:

$$\sigma_y = \sigma_0 + k/\sqrt{d} \qquad \text{eq (5.1)}$$

where σ_y stands for the yield strength, σ_0 is the friction stress below which dislocations will not move in the material in absence of grain boundaries, k is a constant and d is the grain size. After a maximum of strength and hardness around 10 nm, an inverse Hall-Petch behaviour is observed for smaller grain sizes.

Table 5.1 shows also that with the reduction of the grain size the ductility is negatively influenced, especially tensile ductility. The tensile elongation to fracture, still in the range of 15% for grain sizes between 50-100 nm, drastically drops below 1% at grain sizes of 10 nm. Greater ductility however was observed during bending and cold rolling[34], which best suits the kind of application for the Hybrix^{TM} material. Different attempts have been made to enhance the low ductility of nanocrystalline nickel. One suggested strategy for enhancing ductility in nanometals is to develop a bimodal grain size distribution, in which fine grains yields to high strength while coarse grain can enable strain hardening to enhance ductility[39]. However this strategy hasn't always proved to be effective[40]. An improvement can be obtained through the addition of second-phase particles in the nanocrystalline matrix. Adding SiC particles has proven to increase the ductility of nanocrystalline nickel of 10 nm grain size from 0.6% up to 2.1%[34], see figure 5.1. The obtained tensile ductility is still far from the value of a regular polycrystalline nickel, but it is in the same range of the corresponding Ni-SiC composite, but in addition with a greater yield strength and hardness at a lower concentration of SiC particles.

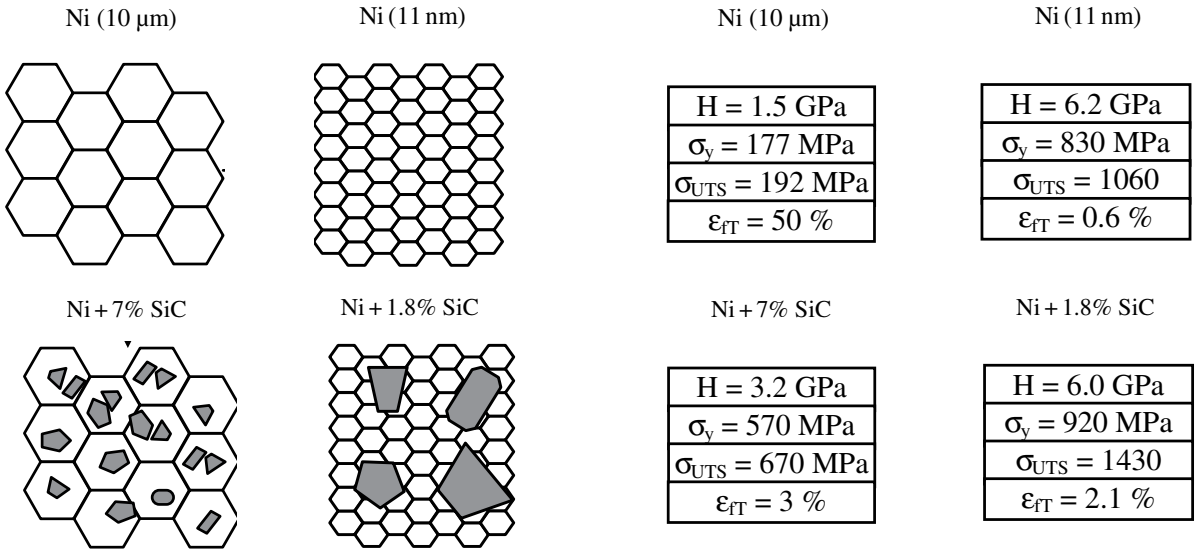

Figure 5.1: Comparison of hardness (H), yield strength (σ_y), ultimate tensile strength (σ_{UTS}), and elongation to fracture (ε_{UT}), for conventional and nanocrystalline nickel, and for conventional and nanocrystalline Ni-SiC composite[34].

5.3 Previous work on Ni electrodeposition

In this paragraph, the influence of the different electroplating parameters on the characteristics of the final electrodeposited component (grain size, grain size distribution, texture, surface appearance, etc.) will be discussed in more detail. Many parameters can be changed in order to have a deposited material with a certain microstructure. Furthermore the mechanism behind some obtained results under certain condition is still not fully understood. Hence, it is difficult to have a generic description of all the possible effects obtained varying freely the plating conditions. For this reason, studies described in literature dealing with plating conditions similar to the ones intended in this project will be discussed.

The most relevant electrodeposition parameters are the following: type of electrolyte used, pH of the solution, deposition current (direct or pulsed, and in this case which pulse function), additives present in the solution (grain refining or wetting agents), solution temperature, as well as solution filtering. The two most common electrolyte solutions are the Watt's-type and the sulfamate electrolyte solution. The basic composition of these two bath electrolytes is listed in the tables in fig 5.2. The main difference between the two solutions is related to the concentration of Ni^{2+} in the aqueous solution, whose higher concentration facilitates the deposition of a dense material. In both solution types the boric acid is the pH-controlling agent. The recommended pH level for electrochemical deposition processes ranges between 3.5-4.5. It has also been reported that after several hours of deposition the pH level of the bath tends to change from the initial value. Hence, a proper control of the pH value over time is then required. As already mentioned in the previous paragraph, the deposition current density plays a fundamental role in the control of the predominant deposition mechanism (new nuclei formation or growth of an existing grain).

Watt's bath

Chemical Name	Formula
Nickel sulfate	$NiSO_4 \cdot 6H_2O$
Nickel chloride	$NiCl_2 \cdot 6H_2O$
Boric acid	H_3BO_3

Sulfamate bath

Chemical Name	Formula
Nickel sulfamate	$Ni(SO_3NH2)_2$
Nickel chloride	$NiCl_2 \cdot 6H_2O$
Boric acid	H_3BO_3

Figure 5.2: Basic composition of Watt's and sulfamate elocrolyte solutions

Generally, high current densities lead to formation of smaller grains. This condition can be achieved by using pulse current, where the peak of the current density can be considerably higher than the current obtained during direct current plating[34]. A graphical representation of a general set up for pulse electrodeposition is showed in figure 4.

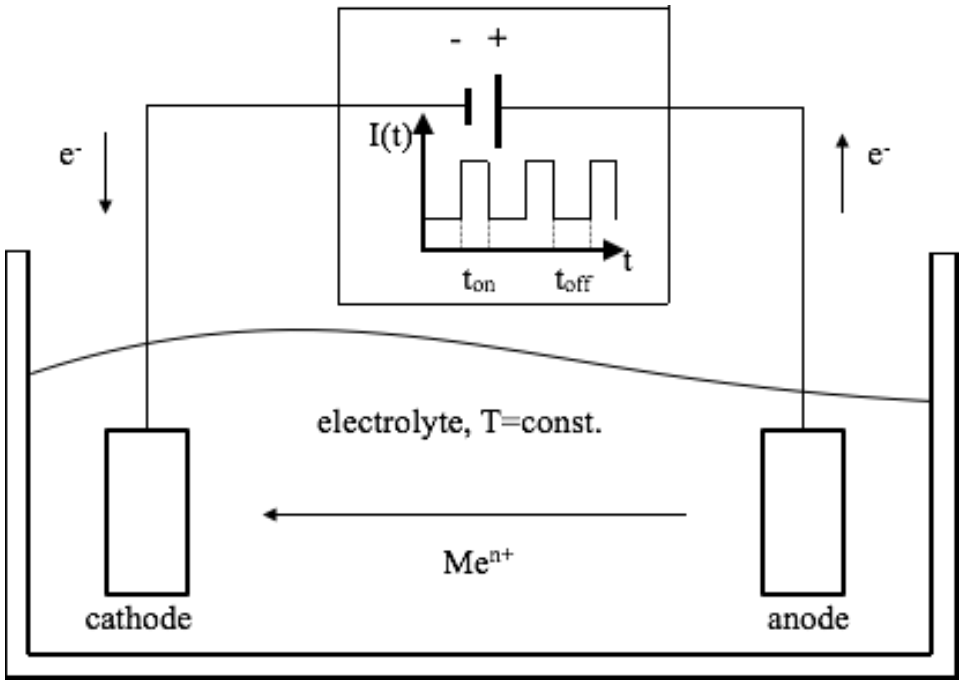

Figure 5.3: Schematic illustration of pulse electrodeposition set up

The effect of the applied current has been studied as well by Shüller et al.[41]. Their results show clearly how smaller grains are obtained switching from direct current to pulse current. They show also how at higher current densities a linear decrease of the grain sizes is obtained.

In the same paper, the influence of other parameters like the pulse function (t_{on}, t_{off}) and grain refinement additives is studied. The results obtained in this study reveal the need of grain refining agents in order to obtain nanocrystalline grains. The grain refinement agents limit the grain growth by segregating at the grain boundaries. However, their addition can also alter the crystallographic orientation. Grain refiners can on one hand be organic, butynediol and saccharin are common examples, but on the other hand, interesting results have also be obtained using metallic grain refiners such as manganese or magnesium chloride. Other types of additives that can be added to the basic electrolytic solution composition are wetting agents.

An interesting analysis of the influence of applied current densities and electrolyte solution temperature on the microstructure of electrodeposited nickel was performed by Goods et al.[42]. They also analysed the effect of a filtering system for the electrolyte solution. Mechanical tests, tensile elongation in particular, were performed on the electrodeposited nickel material, in order to assess its mechanical properties in correlation to the obtained texture. Two different nickel microstructures were obtained under the different deposition condition investigated. In one case, the main crystallographic orientation of the obtained grains was⟨001⟩. The other case showed instead the obtained texture was ⟨101⟩. The deposition parameters applied by Goods et al. are really similar to those used in this project. As it will be seen in the following paragraph, the microstructure of the obtained nickel layer is characterized by the same crystallographic orientation, ⟨001⟩.

5.4 Nickel deposition: experimental procedure

In this project, pulsed-electrodeposition with a sulfamate bath is performed. The whole operating device and the operating conditions are showed in figure 5.4. The samples for the deposition were rectangular stainless steel sheets (2x6 cm) cut from a stainless steel panel thick 0,2 mm, provided by Lamera AB. The only pre-treatment performed on the samples was a cleaning with a regular detergent in order to avoid any contamination of organic species on the metal surface. The cleaned samples were then attached to the cathode through conventional rubber tape. In figure 5.5 are showed in detail the steel plate cathode, the nickel pellets used as anode and a voltmeter used to check the conductivity between the cathode and the stainless steel sample.

After the deposition, cleaning was performed through ethanol rinsing, followed by further ultrasonic cleaning for 5-10 minutes. The nickel layer was then peeled off from the metallic substrate using a razor and tweezers, and its integrity was controlled through optical microscope.

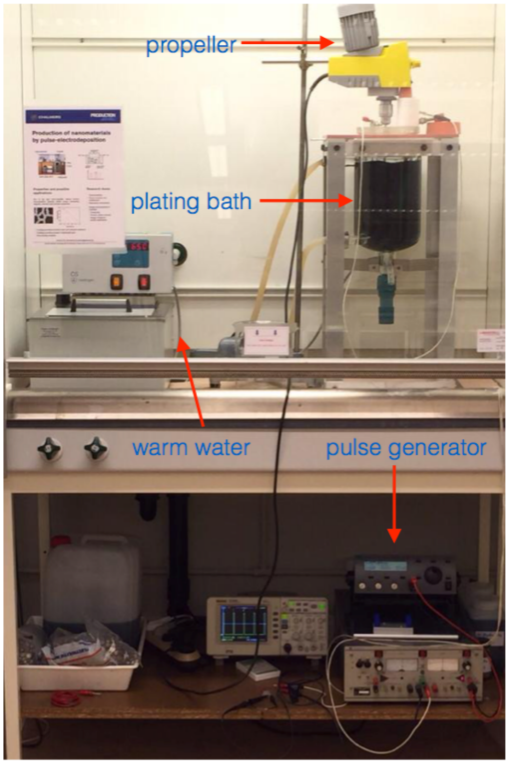

Bath volume	2 litres
Bath temperature	65°C
pH	≈4
Pulse form	rectangular
t_{on}	5 ms
t_{off}	45 ms
Pulse current	12,5 mA/cm^2
Anode	Ti basket with Ni pellets
Cathode	Steel plate of 4x7 cm^2
Distance anode-cathode	6 cm

Figure 5.4: Pulse-electrodeposition device on the left, plating conditions on the right

Three different deposition times were first investigated to determine the obtained coating thicknesses: one hour, two hour, and six hours. To have a sufficiently thick nickel layer for the surface analysis, the samples deposited for six hours were investigated. In this case the obtained nickel film had a thickness of about 40-45 µm. In figure 5.6 is showed the nickel layer, peeled off from it's substrate, after six hours of deposition.

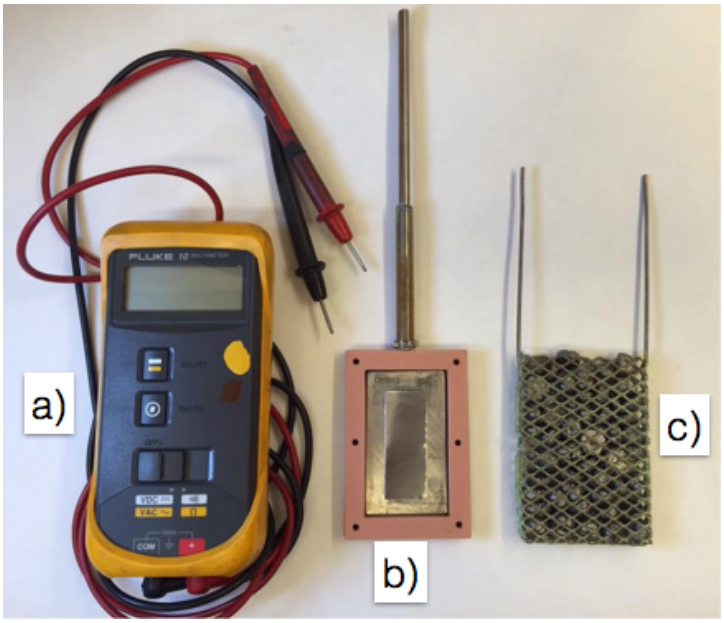

Figure 5.5: Image showing the voltmeter to check the conductivity (a), the cathode (b), and the nickel basket used as anode (c)

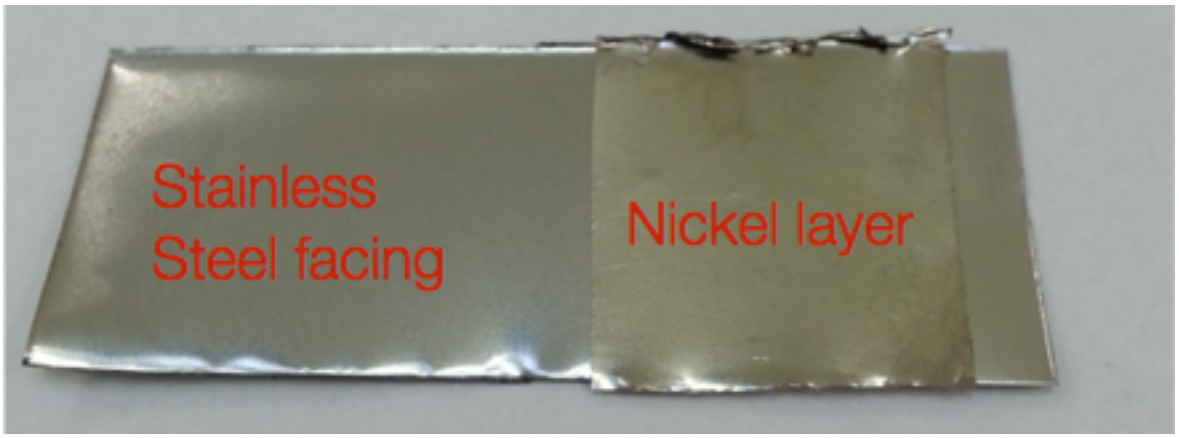

Figure 5.6: Hybrix^{TM} stainless steel facing and the nickel layer obtained after 6 hours of deposition

5.5 Surface characterization

For the surface characterization of the nickel foil two different techniques were used, scanning electron microscope (SEM) coupled with electron backscatter diffraction (EBSD) technique was used for the analysis of the grain size distribution and of their crystallographic orientation. Transmission electron microscopy (TEM), for a more accurate analysis of the smallest grains evaluated during the SEM and EBSD measurements.

In SEM analysis, the electron beam has an accelerating voltage much lower compered to the one in the TEM. For this reason and for a lower lateral resolution always in comparison with TEM, SEM is usually not suitable for the investigation of nanocrystalline materials. However, the SEM has the advantage of providing microstructure and texture informations by using the EBSD technique. Furthermore, for statistical evaluation, a larger number of grains can be investigated as compared to TEM analysis[43]. Since the diffracted electrons that produce the pattern for the microstructure analysis escape from top 10-20 nm of the surface, a highly polished, flat surface is required. Due to the low thickness of the nickel films, samples for the microstructure investigation were obtained through electrolyte polishing instead of the more common mechanical polishing. A LECTROPOL-5 with an A2 electrolyte solution was used. For each sample a voltage of 31 V for 10 seconds was applied.

The polished samples were first investigated in a Leo 1550 Gemini FEG-SEM, tilted of 70° towards the EBSD detector. This procedure is applied in order to reduce the path length of the backscattered electrons and thus to enhance the signal by ensuring the maximum diffraction of the electrons[44]. To collect the grains orientation map, the electron beam scans the surface of the sample in a regular pattern, with a chosen step size. At each step the EBSD software indexes the obtained pattern by a comparison with the crystallographic data of the expected phase. If for any reason the indexing in not possible (an undefined phase, poor pattern quality, overlapping patterns from adjacent grains) the obtained pixel is non-indexed, and referred as a “zero solution” pixel[44].

The obtained orientation maps were finally analysed using an HKL Channel 5 EBSD system in order to obtain information such as texture and grain size distribution. The orientation maps are showed in figure 5.7, the grain size histogram instead in figure 5.8.

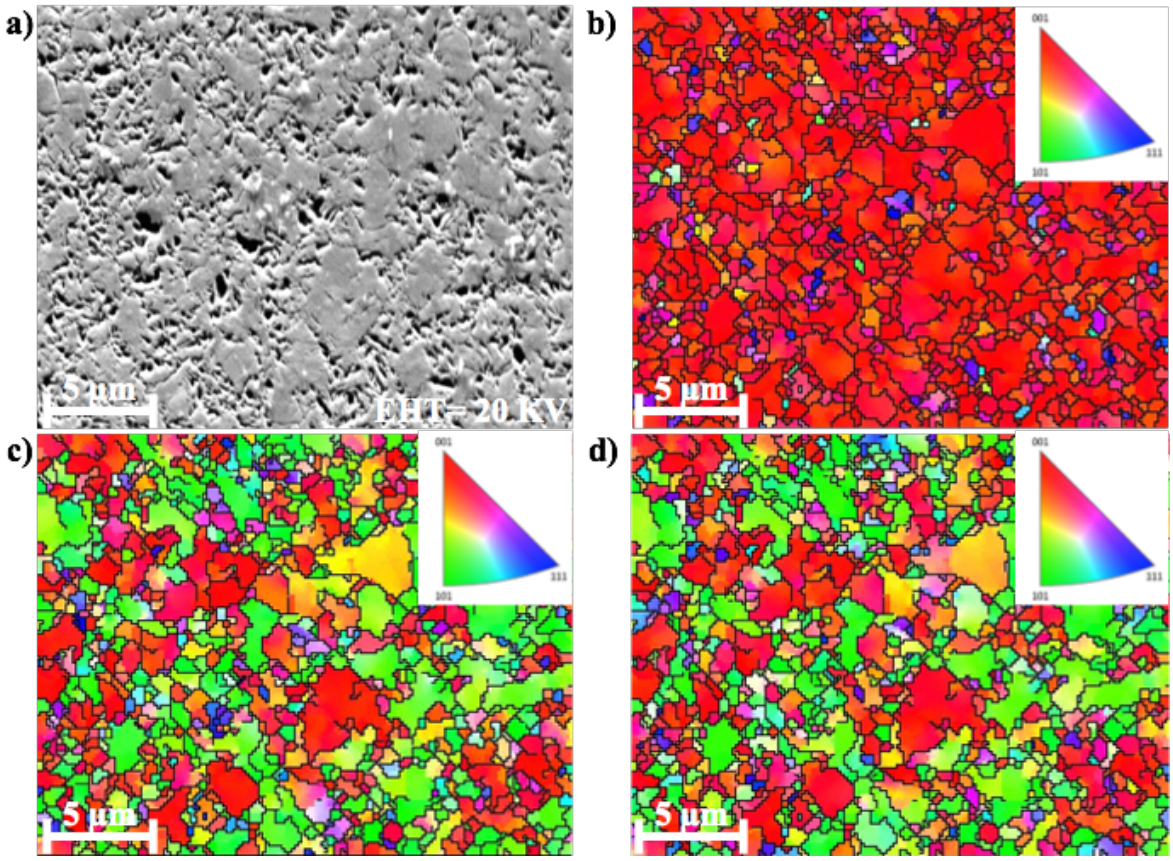

Figure 5.7: EBSD image of the nickel surface area analysed (a), orientation map in inverse pole figure colouring along z-axis (b), orientation map in inverse pole figure colouring along x-axis (c), orientation map in inverse pole figure colouring along y-axis (d)

To obtain a better evaluation of the smaller grains, a Zeiss EM 912 Omega TEM microscope with a LaB_6 electron gun was used. Besides the higher accelerating voltage applied with respect to SEM, here the electron beam passes through the sample and some of the incident electrons interact with the atoms in the sample and are diffracted while other electrons are transmitted without diffraction. Selecting the transmitted beam a bright-field image is obtained, using the diffracted electron a dark-field image is achieved instead[43]. The sample preparation for TEM analysis was different from the one previously described. Here the nickel film was cut and glued in a copper TEM sample holder of 2x1 mm. Ion milling was performed on both sides of the disc with a Gatan ion polishing system using an angle of incidence of 4° until a hole was created in the centre of the sample. The obtained TEM micrographs are shown in figure 5.9.

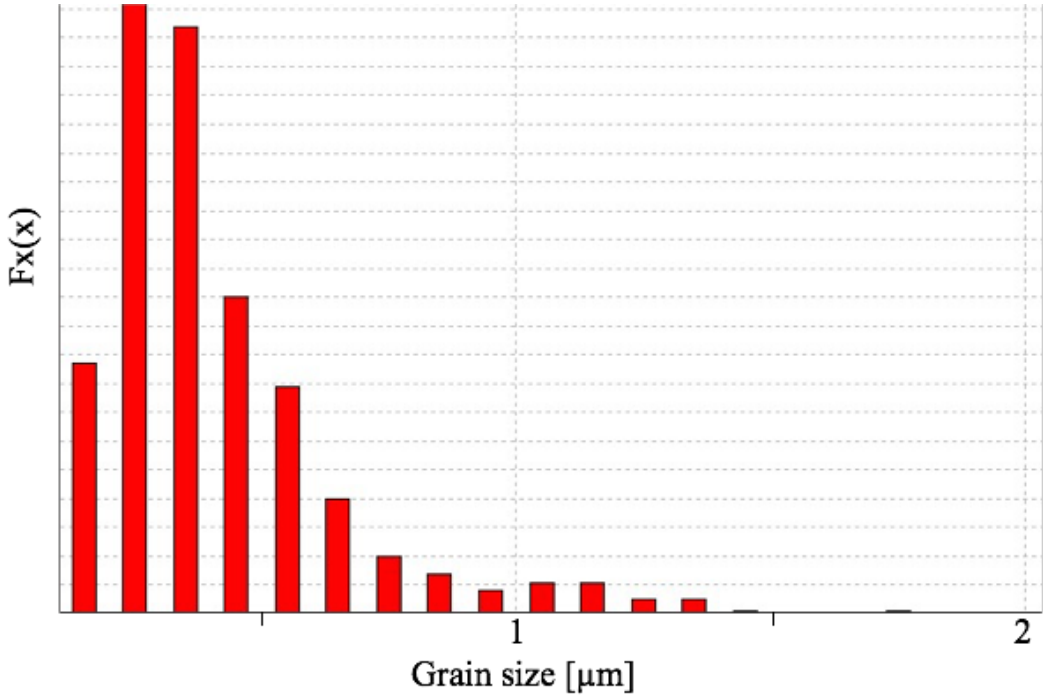

Figure 5.8: Nickel grain size histogram

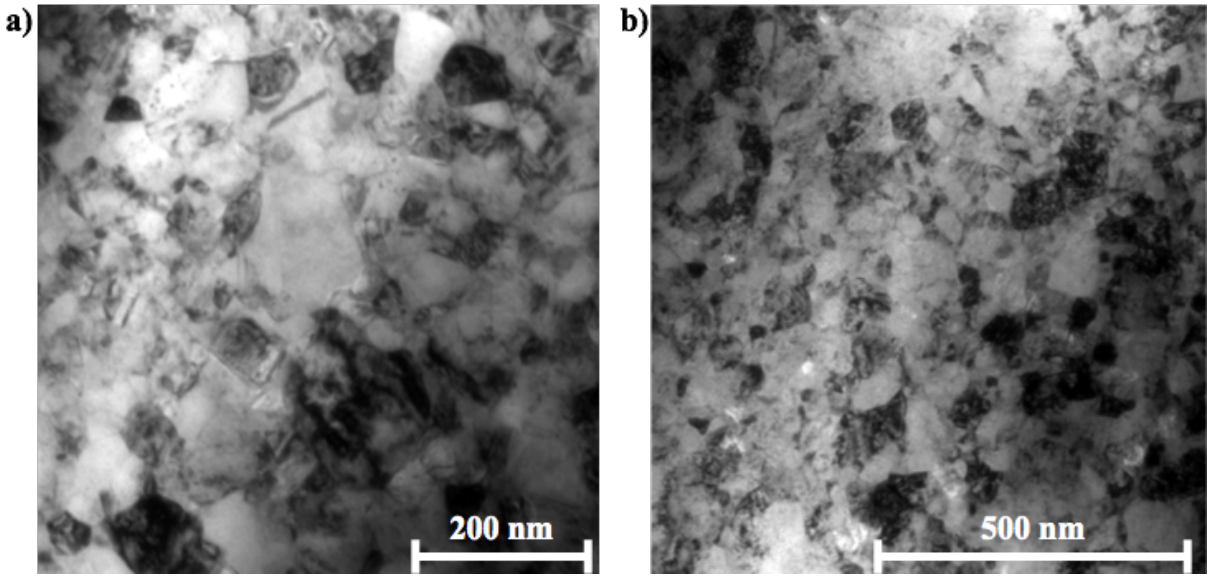

Figure 5.9: TEM micrographs obtained at different magnification of the electrodeposited nickel layer

5.6 Nanoindentation test

In order to assess the Vickers hardness of the electrodeposited nickel layer analysed in paragraph 5.5, nanoindentations tests have been performed. The tests were performed at Kaiserslautern University of Technology, Germany. The nickel, whose surface characterization is shown in figure 5.7, was the sample tested. A piece of the nickel layer was cut and glued in an appropriate sample holder, as showed in fig 5.10.

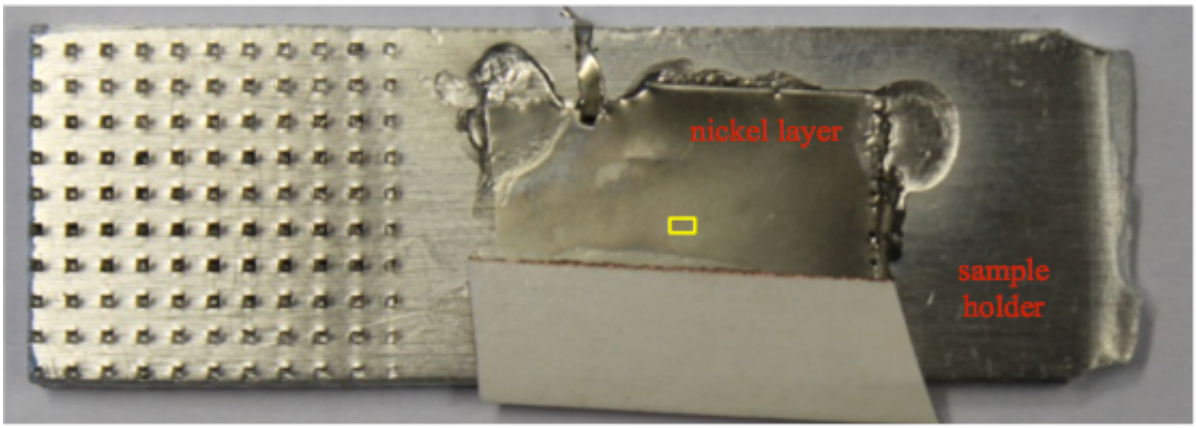

Figure 5.10: Nickel layer attached to the sample holder for nanoindentation tests

The yellow area present in fig 5.10, within the nickel layer, shows the area where the indentations were performed. In particular two areas of 50x90 µm were indented with two different loading forces: i.e. one with 1 mN, the other with 5 mN. Figure 5.11 shows the indented areas with the two forces, and the corresponding hardness distribution values, measured in kg/mm^2. The area market with the blue corner represents the sample area indented and the hardness values obtained with 5 mN force. The red corner stands instead for the 1mN. Some of the measurements done with 1 mN force weren't possible to be analysed, and this explains the missing hardness data showed in figure 5.11 (a).

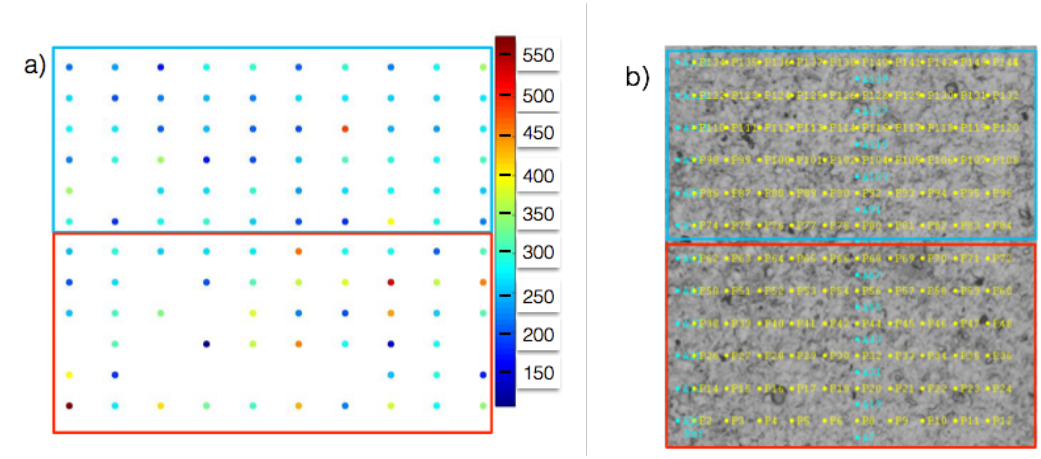

Figure 5.11: Distribution of the measured hardness values (a), sample's indented areas (b)

The histograms of the hardness values showed in figure 5.11 are also here presented:

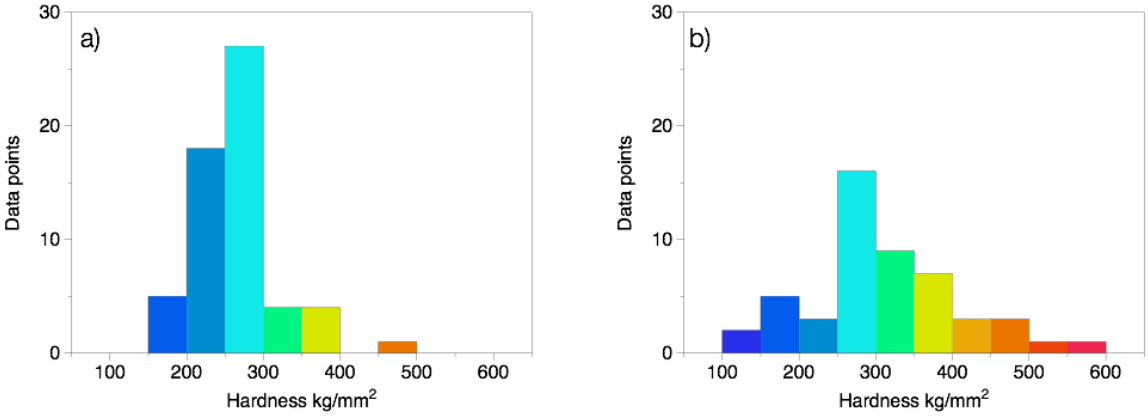

Figure 5.12: Hardness values histogram of the values obtained with 5 μN loading force a), and with 1 μN loading force b)

5.7 Surface characterization and nanoindentation test: discussions and conclusions

The results obtained from the surface characterization of the electrodeposited nickel layer yield to several conclusions. As it appears form the EBSD analysis the grain size distribution is not uniform. The presence of larger grains surrounded by other smaller grains is observed. However, from the grain size histogram it appears how the bigger grains are in a few numbers. Most of the grain sizes are registered below 500 nm, the majority in particular characterized with a grain size between 250-400 nm. TEM micrographs show furthermore the probable presence of grains with dimension smaller than 100 nm. From the hardness measurement histograms, showed in fig. 5.12, this not uniform distribution of grain sizes seems to be confirmed.

Most of the measured hardness values are in the range between 200-300 kg/mm^2. These are expected values for an electrodeposited nickel structure with grain size ranging around 100 μm, see table 5.2. Regarding the texture of the obtained nickel layer, the orientation maps, reported in fig. 5.7, show a strong preferential orientation of the grains towards the grain growth direction, ⟨001⟩-texture.

Property	Hybrix^{TM} stainless steel facing	Conventional nickel	Nano-nickel (100 nm)	Nano-nickel (10 nm)
Vickers hardness, kg/mm^2	148	140	300	650

Table 5.2: Hardness values for Hybrix^{TM} stainless steel facing and of nickel with different grain sizes

As an attempt to obtain nanocrystalline metallic coating through pulse-electrodeposition useful information have been obtained. The plating parameters are not optimized for obtaining nanocrystalline grains. Further investigation regarding plating parameters is needed in order to reach grains with dimensions in the nanoscale, and homogeneously distributed. However, with the applied plating conditions submicron grain sizes are obtained.

Regarding the possibility to enhance properties of lightweight structures, the obtained hardness value of the nickel layer are higher than the hardness of the Hybrix^{TM} stainless steel facing, see table 5.2. It should me mentioned that only measurements on the nickel layer, separated from the stainless steel facing, were performed. The optimization of the deposited coating is thought to be the first step for then performing test on the overall structure, i.e. composite material with coated facing.

6 Conclusions and future developments

In the present thesis work an ultra-light polymer-metal sandwich composite was studied. The material analysed is produced by Lamera AB, a company working within the production and development of lightweight sandwich materials, operating in Gothenburg, Sweden. This sandwich composite is characterized by two thin metal facing, i.e. aluminium or stainless steel, and a polymeric core of polyamide 6,6 fibres, bonded to the metal facing through an epoxy adhesive layer. The project was entirely developed at the Department of Materials and Manufacturing Technology of Chalmers University of Technology (Gothenburg-Sweden), under the supervision of Dr. Roland Kádár.

In this thesis project a broad characterization of Hybrix^{TM} is performed in three branches: (i) investigation of the thermorheological properties and damping performances of the polymeric core, (ii) bending stiffness and core shear rigidity measurements, (iii) characterization of an electrodeposited nickel metal coating. The main market competitors individuated by Lamera AB for their product are solid metal panels, polymer-based composites, and other light-weight sandwich materials operating in different industry sectors, i.e. automotive and aircraft industry, building, home appliance, electronic goods. The results of the performed test can be useful for the market applications of Lamera AB product.

The most important factor influencing the thermorheological behaviour of the tested sandwich specimens is the type of adhesive used. The specimens investigated were characterized by two different adhesives: (i) a two component epoxy based adhesive with three different mixing ratio of the resin/hardner and (ii) a single component epoxy adhesive. In this project the two different adhesives are respectively referred as adhesive B and adhesive C. The tests performed were dynamic mechanic thermal analysis, DMTA, tests: i.e. temperature ramp and frequency-sweep tests, under three-point bending.

The results allowed the calculation of the different adhesive glass transition temperature, T_g, both from the tan δ peaks and from the intercepts of the storage modulus, E'. The thermorheological properties of polyamide fibres, present in the sandwich core, are not evidenced in the testing conditions applied. Therefore the thermorheological response of the material can be entirely attributed to the polymeric adhesive. All the samples characterized with adhesive B and stainless steel facing suffered delamination. It occurs after reaching temperatures 20-30°C in excess of the measured T_g. In contrast, the adhesive

C samples were not affected by the same problem. Hence a limitation on the reliability for the sandwich material characterized by adhesive B, depending on the operating temperature, is apparent.

As a first step, regarding the investigation of the possible delamination causes, surface roughness measurements for both aluminium and stainless steel facing have been performed. As a matter of fact the main bonding mechanisms occurring between epoxy adhesives and metals are mechanical keying and chemical bonding. Mechanical keying is favoured by rougher surfaces. The test results showed a higher average surface roughness for the aluminium facing, S_a=0,27 μm, with respect of the stainless steel facing, S_a=0,18 μm.

The damping performance was investigated for both adhesives through temperature-frequency sweeps. To enlarge the investigated frequency range, the time-temperature superposition principle (TTS) was tested. The analysed sample with adhesive B showed a non-optimal overlapping of the viscoelastic properties in the built mastercurve. The adhesive C shows a better applicability of the TTS for the obtained mastercuve with respect of the adhesive T_g. The damping properties of the Hybrix^{TM}, obtained from variation of the loss factor with frequency, show to be strongly dependent on the temperature. For high temperatures, close to the adhesive T_g, the loss factor for the adhesive C reaches values competitive with those of amorphous polymers, commonly used for high damping materials.

To measure the mechanical properties static bending tests were conducted with a 3-point bending loading fixture. From the tests results the bending stiffness for different Hybrix^{TM} configurations was measured. In addition, a first evaluation of the material core shear modulus was obtained through a first-order shear analysis. The average values of the shear modulus are higher (between 138-109 MPa for adhesive B samples, 224 for adhesive C samples) than other common polymeric foam-core materials. This can be attributed to the presence of the nylon fibres, acting as through thickness reinforcement. Still from the measured values it appears that adhesive C is characterized by the highest shear stiffness. This result strengthens the better mechanical performances of the adhesive C, also at room temperature.

As a possibility to enhance the properties of lightweight materials, the electrodeposition of a nickel metal layer was performed and analysed. Nickel layers were obtained through

pulse-electrodeposition with a sulfamate electrolytic bath. Surface characterization tests, electron back-scattered diffraction (EBSD) and transmission electron microscopy (TEM) analyses were performed in order to assess the microstructural features (i.e. grain size, grain size distribution and texture) of the electrodeposited nickel layers. The resulting EBSD micrographs show that the obtained nickel is characterized mostly by submicron grain sizes, the majority fall below 500 nm. These are characterized by a strong crystallographic orientation along the grain growth direction. However the grain size distribution is not homogenous. Few bigger grains are present, with dimensions around 1,5 μm. TEM analysis shows also some areas characterized by grains probably smaller than 100 nm.

Vickers hardness measurements seem to confirm this distribution of nickel grain sizes. The obtained values, mostly between 200-300 kg/mm^2, are in fact in the range of expected hardness values for a nickel electrodeposited material with grain size ranging between 0,1-1 μm. These values represent already an improvement of the hardness values of the Hybrix^{TM} stainless steel facing, 148 kg/mm^2. Higher performances can be obtained by the optimization of the nickel coating.

Numerous future developments stemming from the present study can be envisioned. An investigation of the possible strategies to avoid the facing delamination, occurring using adhesive B. Different surface treatments of the stainless steel facing, to increase roughness and wettability of the adhesive layer can be investigated. Regarding the electrodeposition of a protective metal coating an optimization of the plating parameters may be of interest. This can lead to homogeneous nanocrystalline structures.

References

[1] R. F. Gibson, *Principle of Composite Materials Mechanics*. McGraw-Hill, Inc., 1994.

[2] M. F. Ashby and Y. J. M. Bréchet, "Designing hybrid materials," *Acta Mater.*, vol. 51, no. 19, pp. 5801–5821, 2003.

[3] E. Hammel, X. Tang, M. Trampert, T. Schmitt, K. Mauthner, a. Eder, and P. Pötschke, "Carbon nanofibers for composite applications," *Carbon N. Y.*, vol. 42, no. 5–6, pp. 1153–1158, 2004.

[4] D. Gay, S. V. Hoa, and S. W. Tsai, *Composite Materials: Design and Application*. CRC Press, 2003.

[5] D. Hull and T. W. Clyne, *An Introduction to Composite Materials*, 2nd Edition. Cambridge University Press, 1996.

[6] J. W. Kaczmar, K. Pietrzak, and W. Wlosinski, "The production and application of metal matrix composite materials," *J. Mater. Process. Technol.*, vol. 106, no. 1–3, pp. 58–67, 2000.

[7] H. Ohnabe, S. Masaki, M. Onozuka, K. Miyahara, and T. Sasa, "Potential application of ceramic matrix composites to aero-engine components," *Compos. Part A Appl. Sci. Manuf.*, vol. 30, no. 4, pp. 489–496, 1999.

[8] L. A. Carlson and G. A. Kardomateas, *Structural and Failure Mechanics of Sandwich Composites*. 2011.

[9] L. B. Vogelesang, "Development of a New Hybrid Material (ARALL) for Aircraft Structure," no. Figure 3, pp. 492–496, 1983.

[10] L. B. Vogelesang and J. W. Gunnink, "ARALL: A materials challenge for the next generation of aircraft," *Mater. Des.*, vol. 7, no. 6, pp. 287–300, Nov. 1986.

[11] O. a. Pawar, Y. S. Gaikhe, A. Tewari, R. Sundaram, and S. S. Joshi, "Analysis of hole quality in drilling GLARE fiber metal laminates," *Compos. Struct.*, vol. 123, no. 2015, pp. 350–365, 2015.

[12] "Compendium Composite and nanocomposite materials, Ed. 6, 2012 compiled in the Department of Materials and Manufacturing Technology, Chalmers." pp. 1–75.

[13] "Hybrix^{TM} brochure". June 2014.

[14] J. Wingborg, "Product development of Lightweight Sandwich Material," Chalmers University of Technology, Gothenburg, Sweden, 2011.

[15] M. Grujicic, V. Sellappan, M. a. Omar, N. Seyr, A. Obieglo, M. Erdmann, and J. Holzleitner, "An overview of the polymer-to-metal direct-adhesion hybrid

technologies for load-bearing automotive components," *J. Mater. Process. Technol.*, vol. 197, no. 1–3, pp. 363–373, 2008.

[16] T. A. Osswald and G. Menges, *Material Science of Polymers for Engineers,* 3rd Edition. 2012.

[17] G. Li, G. Li, P. Lee-Sullivan, and P. Lee-Sullivan, "Determinatin of activation energy for glass transition of an epoxy adhesive using DMA," *J. Therm. Anal. Calorim.*, vol. 60, pp. 377–390, 2000.

[18] E. Vaca-cortés, M. A. Lorenzo, J. O. Jirsa, H. G. Wheat, and R. L. Carrasquillo, "Adhesion testing of epoxy coatings," *Cent. Transp. Res. Bur. Eng. Res. Univ. Texas Austin*.

[19] M. Nakazawa, "Mechanism of adhesion of epoxy resin to steel surface," 1994.

[20] Y. Xu, Q. Wu, Y. Lei, and F. Yao, "Creep behavior of bagasse fiber reinforced polymer composites," *Bioresour. Technol.*, vol. 101, no. 9, pp. 3280–3286, 2010.

[21] C. W. Feng, C. W. Keong, Y. P. Hsueh, Y. Y. Wang, and H. J. Sue, "Modeling of long-term creep behavior of structural epoxy adhesives," *Int. J. Adhes. Adhes.*, vol. 25, no. 5, pp. 427–436, 2005.

[22] M. Tajvidi, R. H. Falk, and J. C. Hermanson, "Time-temperature superposition principle applied to a kenaf-fiber/high-density polyethylene composite," *J. Appl. Polym. Sci.*, vol. 97, no. 5, pp. 1995–2004, Sep. 2005.

[23] E. J. L. J. Zhang, R. J. Perez, "Documentation of damping capacity of metallic, ceramic and metal-matrix composite materials," *J. Mater. Sci.*, vol. 28, pp. 2395–2404, 1993.

[24] M. D. Rao, "Recent applications of viscoelastic damping for noise control in automobiles and commercial airplanes," *J. Sound Vib.*, vol. 262, no. 3, pp. 457–474, 2003.

[25] J. G. V.-V. R.E. Wetton, R.D.L. Marsh, "Theory and application of dynamic mechanical thermal analysis," *Thermochim. Acta*, vol. 5, no. 1391, pp. pp. 1–11, 1991.

[26] J. D. Ferry, *Viscoelastic Properties of Polymers*, 3rd Edition. 1980.

[27] J. Dealy, D. Plazek "Time-Temperature Superposition- A Users Guide." *Rheo. Bull,* vol. 2, pp. 16-21, 2009.

[28] C. G. Robertson and C. M. Rademacher, "Coupling model interpretation of thermorheological complexity in polybutadienes with varied microstructure," *Macromolecules*, vol. 37, no. 26, pp. 10009–10017, 2004.

[29] J. P. Szabo and I. a Keough, “Method for analysis of dynamic mechanical thermal analysis data using the Havriliak - Negami model,” *Thermochim. Acta*, vol. 393, pp. 392–393, 2002.

[30] H. Oberst, “Reduction of noise by the use of damping materials,” *Philos. Trans. R. Soc. London*, pp. 441–453, 1969.

[31] a. F. Johnson and G. D. Sims, “Mechanical properties and design of sandwich materials,” *Composites*, vol. 17, no. 4, pp. 321–328, Oct. 1986.

[32] E. M. Reis and S. H. Rizkalla, “Material characteristics of 3-D FRP sandwich panels,” *Constr. Build. Mater.*, vol. 22, no. 2008, pp. 1009–1018, 2008.

[33] K. Lingaiah and B. G. Suryanarayana, “Strength and stiffness of sandwich beams in bending,” *Exp. Mech.*, vol. 31, no. 1, pp. 1–7, 1991.

[34] C. C. Koch, *Nanostructured Materials, Second Edition*. 2007.

[35] H. Natter, M. Schmelzer, R. Hempelmann, and I. Introduction, “Nanocrystalline nickel and nickel-copper alloys: Synthesis, characterization, and thermal stability,” *J. Mater. Res.*, p. pp 1186–1197, 1998.

[36] J. O. Bockris and G. A. Razumney, *Fundamental Aspects of Electrocrystallization*. Plenum Press, 1967.

[37] W. H. Safranek, *The Properties of Electrodeposited Metals and Alloys, 2nd edition*. 1986.

[38] Y. Lu and P. K. Liaw, “The mechanical properties of nanostructured materials,” *Jom*, vol. 53, pp. 31–35, 2001.

[39] Y. Wang, M. Chen, F. Zhou, and E. Ma, “High tensile ductility in a nanostructured metal.,” *Nature*, vol. 419, no. 6910, pp. 912–915, 2002.

[40] M. J. N. V Prasad, S. Suwas, and a. H. Chokshi, “Microstructural evolution and mechanical characteristics in nanocrystalline nickel with a bimodal grain-size distribution,” *Mater. Sci. Eng. A*, vol. 503, no. 2009, pp. 86–91, 2009.

[41] K. Schüler, B. Philippi, M. Weinmann, V. M. Marx, and H. Vehoff, “Effects of processing on texture, internal stresses and mechanical properties during the pulsed electrodeposition of nanocrystalline and ultrafine-grained nickel,” *Acta Mater.*, vol. 61, pp. 3945–3955, 2013.

[42] S. H. Goods, J. J. Kelly, a. a. Talin, J. R. Michael, and R. M. Watson, “Electrodeposition of Ni from Low-Temperature Sulfamate Electrolytes,” *J. Electrochem. Soc.*, vol. 153, p. C325, 2006.

[43] M. Da Silva, “Thermal Stability of Electrodeposited Nanocrystalline Ni- and Co-Based Materials.pdf,” Chalmers University of Technology, Gothenburg, Sweden, 2007.

[44] K. P. Mingard, B. Roebuck, E. G. Bennett, M. G. Gee, H. Nordenstrom, G. Sweetman, and P. Chan, “Comparison of EBSD and conventional methods of grain size measurement of hardmetals,” *Int. J. Refract. Met. Hard Mater.*, vol. 27, no. 2, pp. 213–223, 2009.